Constraining Precipitation Susceptibility of Warm-, Ice-, and Mixed-Phase Clouds with Microphysical Equations

FRANZISKA GLASSMEIER[a] AND ULRIKE LOHMANN

Institute for Atmospheric and Climate Science, ETH Zürich, Zurich, Switzerland

(Manuscript received 11 January 2016, in final form 27 June 2016)

ABSTRACT

The strength of the effective anthropogenic climate forcing from aerosol–cloud interactions is related to the susceptibility of precipitation to aerosol effects. Precipitation susceptibility $d\ln P/d\ln N$ has been proposed as a metric to quantify the effect of aerosol-induced changes in cloud droplet number N on warm precipitation rate P. Based on the microphysical rate equations of the Seifert and Beheng two-moment bulk microphysics scheme, susceptibilities of warm-, mixed-, and ice-phase precipitation and cirrus sedimentation to cloud droplet and ice crystal number are estimated. The estimation accounts for microphysical adjustments to the initial perturbation in N. For warm rain, $d\ln P/d\ln N < -2\text{aut}/(\text{aut} + \text{acc})$ is found, which depends on the rates of autoconversion (aut) and accretion (acc). Cirrus sedimentation susceptibility corresponds to the exponent of crystal sedimentation velocity with a value of -0.2. For mixed-phase clouds, several microphysical contributions that explain low precipitation susceptibilities are identified: (i) Because of the larger hydrometeor sizes involved, mixed-phase collection processes are less sensitive to changes in hydrometeor size than autoconversion. (ii) Only a subset of precipitation formation processes is sensitive to droplet or crystal number. (iii) Effects on collection processes and diffusional growth compensate. (iv) Adjustments in cloud liquid and ice amount compensate the effect of changes in ice crystal and cloud droplet number. (v) Aerosol perturbations that simultaneously affect ice crystal and droplet number have opposing effects.

1. Introduction

Atmospheric aerosols influence the radiation balance directly by scattering and absorption and indirectly by modulating cloud albedo. The influence of anthropogenic aerosol on clouds constitutes the largest uncertainty in quantifying the anthropogenic forcing of the climate system (Myhre et al. 2013). Aerosols drastically lower the supersaturations required for cloud droplet and ice crystal formation. Changes in aerosol amount and composition affect droplet and crystal number (Boucher et al. 2013). For warm clouds, an increase in the number of droplet-forming aerosols will redistribute the available condensate to more but smaller droplets. The total reflecting surface and cloud albedo are thus increased (Twomey 1974). In cirrus clouds, an increase of ice-nucleating aerosol may shift crystal formation from homogeneous freezing of solution droplets to heterogeneous nucleation of crystals at an aerosol surface. While homogeneous nucleation describes the freezing of solution droplets when reaching high supersaturations with respect to ice at temperatures colder than 235 K, heterogeneous nucleation sets in at lower supersaturations and warmer temperatures and leads to the formation of fewer crystals. Ice-cloud albedo can thus experience an opposite Twomey effect (Kärcher and Lohmann 2003).

Perturbations to droplet and crystal number trigger responses in the cloud and its environment, which may affect overall cloud albedo by changing cloud amount and lifetime. These feedback-type responses comprise dynamical, thermodynamical, radiative or microphysical effects that act locally and/or on the cloud scale and will be referred to as *adjustments* in the following (Stevens and Feingold 2009). Local and especially

Denotes Open Access content.

[a] Current affiliation: Chemical Sciences Division, NOAA/Earth System Research Laboratory, Boulder, Colorado.

Corresponding author address: Franziska Glassmeier, Chemical Sciences Division, NOAA/ESRL, 325 Broadway, Boulder, CO 80305.
E-mail: franziska.glassmeier@noaa.gov

DOI: 10.1175/JAS-D-16-0008.1

microphysical effects occur in any cloudy volume of air, while cloud-scale effects are usually associated with some degree of convection. Adjustments to aerosol-induced changes in droplet and crystal number are tightly linked to precipitation (Stevens and Feingold 2009; Sherwood et al. 2015): Changes in cloud amount and lifetime correspond to changes in precipitation efficiency (i.e., the ratio of integrated precipitation to integrated condensation rate). For fixed condensation rate, the importance of adjustments in determining the cloud-mediated aerosol forcing is thus related to the strength of an aerosol-induced signal in precipitation.

Focusing on cloud microphysical adjustments, Albrecht (1989) argued that smaller droplet sizes reduce precipitation formation by collision–coalescence of cloud droplets and increase the lifetime of warm clouds (classical lifetime effect). In contrast to droplets, crystals can be large enough to leave the cloud by sedimentation. Increasing crystal sizes and sedimentation velocities tend to decrease cloud lifetime. In cirrus clouds, an aerosol-induced transition from homogeneous to heterogeneous ice formation drastically increases crystal size, which may lead to the dissipation of the cloud (Mitchell and Finnegan 2009; Storelvmo and Herger 2014). In mixed-phase clouds, which occur at temperatures between 273 and 235 K and feature regions consisting of droplets and crystals in parallel, crystal size is increased by a glaciation adjustment: As the saturation vapor pressure with respect to ice is lower than that with respect to water, crystals grow at the expense of evaporating droplets when cloud dynamics creates supersaturations in between water and ice saturation. This is known as Wegener–Bergeron–Findeisen (WBF) process (Wegener 1911; Bergeron 1935; Findeisen 1938; Korolev 2007). Aerosol-induced increases in cloud ice lead to a rapid transfer of available cloud liquid onto crystals, that is, the glaciation of a cloud (glaciation indirect effect) (Lohmann 2002; Storelvmo et al. 2008; Lohmann and Hoose 2009). Complete glaciation transforms a mixed-phase into an ice cloud.

Nevertheless, evidence of aerosol-induced changes in precipitation has proven ambiguous and nonrobust (Boucher et al. 2013). Stevens and Feingold (2009) have proposed the notion of clouds as buffered, or resilient, systems, in which a plurality of processes responds in a compensating fashion to perturbations. According to the buffering hypothesis, compensating adjustments prevent the aerosol signal from propagating to precipitation. While processes important for buffering in warm clouds include dynamical adjustments, a range of cloud microphysical processes is available for compensating adjustments in mixed-phase clouds. In addition to the WBF process, mixed-phase precipitation grows from the liquid-phase pathway via collision–coalescence and from collection processes between liquid- and ice-phase hydrometeors (riming) and pairs of ice-phase hydrometeors (aggregation). In agreement with the buffering hypothesis, modeling studies have found compensations of aerosol effects on mixed-phase cloud microphysics (Lohmann 2002; Storelvmo et al. 2008; Lohmann and Hoose 2009; Muhlbauer et al. 2010; Bangert et al. 2011; Seifert et al. 2012; Saleeby and Cotton 2013).

Precipitation susceptibility s has been proposed as a numerically and observationally feasible metric to quantify the coupling strength between aerosol-induced changes in droplet number concentration N_{cl} and changes in precipitation rate P (Feingold and Siebert 2009):

$$s := \frac{d\ln P}{d\ln N_{\mathrm{cl}}} = \left.\frac{\partial \ln P}{\partial \ln N_{\mathrm{cl}}}\right|_{M_{\mathrm{cl}}} + \left.\frac{\partial \ln P}{\partial \ln M_{\mathrm{cl}}}\right|_{N_{\mathrm{cl}}} \frac{d\ln M_{\mathrm{cl}}}{d\ln N_{\mathrm{cl}}}, \quad (1)$$

where M_{cl} denotes cloud liquid water content. Susceptibility may be interpreted as the ratio of relative changes, $d\ln P/d\ln N_{\mathrm{cl}} = (dP/P)/(dN_{\mathrm{cl}}/N_{\mathrm{cl}}) \approx (\Delta P/P)/(\Delta N_{\mathrm{cl}}/N_{\mathrm{cl}})$ such that a 1% increase in droplet number corresponds to an s% change in precipitation. The decomposition on the right-hand side of Eq. (1) follows when interpreting s as the total derivative of a two-dimensional precipitation function $P[N_{\mathrm{cl}}, \ M_{\mathrm{cl}}(N_{\mathrm{cl}})]$, where the two variables are not independent such that M_{cl} can, in turn, be expressed as a function of N_{cl} (cf. Fig. 1). The total derivative corresponds to a power-law approximation (Jiang et al. 2010): $P = cM_{\mathrm{cl}}^{\alpha}N_{\mathrm{cl}}^{\beta} \Rightarrow \ln P = \ln c + \alpha \ln M_{\mathrm{cl}} + \beta \ln N_{\mathrm{cl}} \Rightarrow d\ln P/d\ln N_{\mathrm{cl}} = \beta + \alpha d\ln M_{\mathrm{cl}}/d\ln N_{\mathrm{cl}}$, where the partial derivatives are given by the exponents. The partial derivative, or partial susceptibility, at constant M_{cl} can be interpreted as immediate response in the spirit of the classical lifetime effect. The second term describes the influence of a perturbation in cloud liquid content that occurs along with the change in N_{cl}. If there exists a causal chain of processes resulting in the (log space) correlation of $d\ln M_{\mathrm{cl}}$ and $d\ln N_{\mathrm{cl}}$, $d\ln M_{\mathrm{cl}}$ is an adjustment to $d\ln N_{\mathrm{cl}}$. Correlated changes in M_{cl} and N_{cl} caused by meteorology or meteorology–aerosol covariability (Boucher et al. 2013) illustrate the difficulty in separating aerosol effects from meteorological variability.

The numerical value of s depends on macrophysical properties characterizing the state and regime of the cloud (Feingold and Siebert 2009), specifically on liquid water path (Sorooshian et al. 2009), cloud height (Terai et al. 2012), the importance of autoconversion compared to accretion (Wood et al. 2009; Feingold et al. 2013), and on the absolute value of N_{cl}

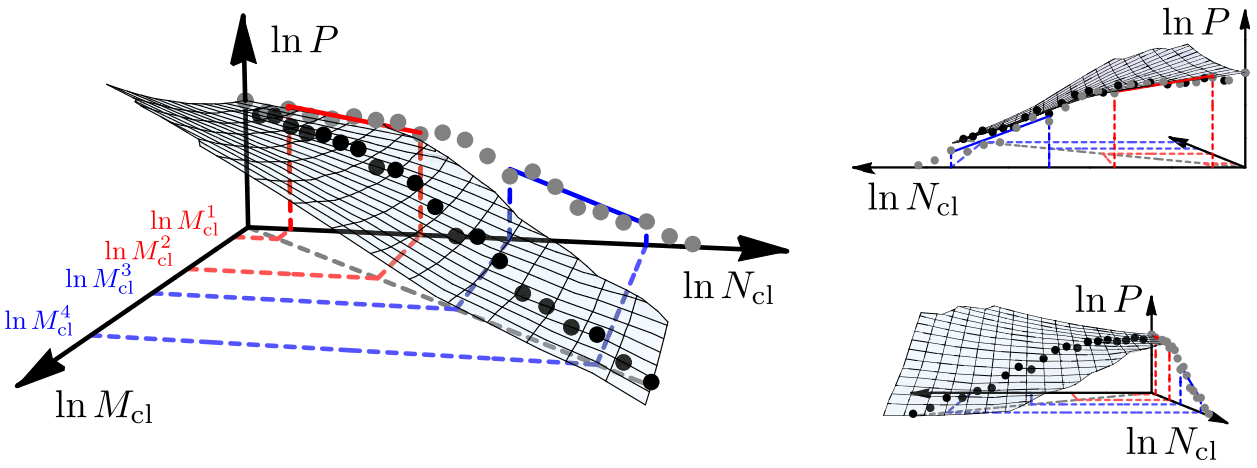

FIG. 1. Illustration of the precipitation susceptibility concept. Warm precipitation rate P is a two-dimensional function of cloud liquid content M_{cl} and droplet number N_{cl} (checkered surface). For fixed M_{cl}, P is assumed to decrease everywhere with increasing N_{cl} as illustrated in the top-right perspective; for fixed N_{cl}, it is assumed to increase with increasing M_{cl} as shown in the bottom-right perspective. For a typical dataset illustrated by black points that scatter about the surface both variables are not independent. The sketch illustrates the special case $\ln M_{cl} \propto \ln N_{cl}$ such that the projection of the data points onto the $\ln N_{cl}$–$\ln M_{cl}$ plane is a straight line (gray dashed line). Any more complicated relationship between N_{cl} and M_{cl} could be locally approximated by such a power-law relationship. Precipitation susceptibility as the total derivative is given by slopes of the projection of the graph of $\ln P(\ln N_{cl}, \ln M_{cl})$ onto the $\ln N_{cl}$–$\ln P$ plane as depicted by the projection of the corresponding data points (gray points). As illustrated in red and blue, slope and susceptibility value are different for different bins (M_{cl}^i, M_{cl}^{i+1}), which specify the macroscopic regimes of the precipitating cloud.

(Feingold et al. 2013). The power-law approximation implied by Eq. (1) thus holds locally, and a possible complexity reduction associated with susceptibilities lies in identifying a limited number of regimes and controlling variables. Figure 1 illustrates the relationship between precipitation susceptibility, M_{cl} and N_{cl}, and the role of regime dependence.

Following Albrecht (1989), warm precipitation susceptibilities are expected to be negative because precipitation decreases for increasing droplet number. This is reflected in a conventional minus sign that has been omitted in our definition in Eq. (1). Warm susceptibility values range from −0.1 to −3.5 (Feingold and Siebert 2009; Lu et al. 2009; Sorooshian et al. 2009; Jiang et al. 2010; Terai et al. 2012; Feingold et al. 2013; Gettelman et al. 2013; Lebo and Feingold 2014; Hill et al. 2015; Terai et al. 2015; Stjern and Kristjánsson 2015), depending on factors mentioned above, exact definitions of variables (Duong et al. 2011), and data resolution (McComiskey and Feingold 2012).

Although more than 90% of precipitation over continents includes ice-phase processes (Mülmenstädt et al. 2015), the susceptibility concept has hardly been applied to cold clouds. In regional modeling studies comprising midlatitude mixed-phase clouds, Bangert et al. (2011) and Seifert et al. (2012) find susceptibilities to droplet number of positive and negative signs with about equal probability. Susceptibilities of precipitation from mixed-phase and ice clouds and sedimentation from cirrus clouds to changes in ice crystal number have, to the authors' knowledge, not been investigated.

Modeling studies that determine values for total derivatives in Eq. (1) quantify effective couplings reflecting the full complexity of adjustment processes in the applied atmospheric model. The partial derivatives in Eq. (1), on the contrary, follow directly from the parameterized equations when evaluated without prior averaging of variables. The equations of cloud microphysics thus already provide constraints for precipitation susceptibility on the level of the parameterization before complex effects from coupling to an atmospheric model emerge. This article is concerned with these cloud microphysical constraints on precipitation susceptibility and does not address dynamical, thermodynamical, or radiative effects.

Many global models feature diagnostic rain and autoconversion parameterizations that follow regime-independent power laws in droplet number and cloud liquid content (Khairoutdinov and Kogan 2000). For these models, partial precipitation susceptibilities are simply given by the autoconversion exponents (Boucher et al. 2013). For schemes with prognostic rain, partial susceptibilities have not been explicitly addressed. In the following, we will derive partial precipitation susceptibilities of warm and mixed- and ice-phase cloud microphysics for the two-moment bulk scheme with prognostic precipitation developed by Seifert and Beheng (2006, hereafter SB) and discuss implications for total precipitation susceptibility s. A modal scheme has the

TABLE 1. Parameter values for Eqs. (2), (8), and (9). Values marked with an asterisk follow the current implementation of the scheme in the COSMO model (Noppel et al. 2010) and differ from SB.

x	a_x (m kg$^{-b_x}$)	b_x	α_x (m s^{-1} kg$^{-\beta_x}$)	β_x	σ_x	ν_x	μ_x
cl	0.124	1/3	3.75×10^{-5}	2./3.	0	0*	1/3*
pr	0.124	1/3	114.*	0.234*	0	0*	1/3
ci	0.835*	0.390*	27.7*	0.216*	0.0625*	0*	1/3
ps	2.4*	0.455*	8.8*	0.150*	0.0625*	0*	1/5*
pg	0.142*	0.314*	86.9*	0.268*	0	1.	1/3

advantage of allowing an analytical treatment as compared to a more realistic bin scheme. We choose the modal SB scheme because its microphysical conversion rates are derived from the stochastic collection equation and because it is validated against the operational version of the numerical weather prediction model of the Consortium for Small-Scale Modeling (COSMO) (Baldauf et al. 2011).

The remainder of the article is structured as follows: In section 2 we summarize the SB microphysics scheme as far as it is relevant for analytically deriving partial precipitation susceptibilities and their sensitivity to adjustments in section 3. In section 4, results from section 3 are applied to estimate total precipitation susceptibilities of warm-, mixed-, and ice-phase clouds. We conclude with section 5. An earlier version of this work is a part of the doctoral thesis of Franziska Glassmeier (Glassmeier 2016).

2. Seifert and Beheng two-moment cloud microphysics

The SB microphysics scheme considers mass and number concentration, M and N, respectively, as two moments that characterize hydrometeor-size distributions:

$$\Gamma(x) = Ax^{\nu_x}\exp(-\lambda x^{\mu_x}) \tag{2}$$

(parameters μ_x and υ_x are given in Table 1). Seifert and Beheng distinguish five hydrometeor types denoted by indices x = cl and x = ci for cloud liquid and cloud ice and x = pr, x = ps, and x = pg for precipitation-sized hydrometeors in the forms of rain, snow, and graupel. Appendix B provides a list of symbols. As prefactors that do not depend on hydrometeor moments drop out in the logarithmic derivative of precipitation susceptibility, we neglect them in the following summary of SB parameterizations.

a. Liquid phase: Autoconversion and accretion

Adopting the nomenclature of SB, liquid-phase precipitation formation proceeds via autoconversion, the collision–coalescence of two hydrometeors in the cloud droplet category resulting in a raindrop, and accretion, denoting the collection of cloud droplets by raindrops. Diffusional growth of liquid-phase hydrometeors is not efficient to reach precipitable sizes and not relevant in this context.

Following the presentation in Stevens and Seifert (2008), the mass transfer from autoconversion is given by

$$\begin{aligned}\mathrm{aut}(M_{\mathrm{cl}}, M_{\mathrm{pr}}, N_{\mathrm{cl}}) &= -\frac{\partial M_{\mathrm{cl}}}{\partial t} = \frac{\partial M_{\mathrm{pr}}}{\partial t} \\ &\propto M_{\mathrm{cl}}^4 N_{\mathrm{cl}}^{-2} \Phi_{\mathrm{cc}}[\varepsilon(M_{\mathrm{cl}}, M_{\mathrm{pr}})]\end{aligned} \tag{3}$$

and for accretion by

$$\mathrm{acc}(M_{\mathrm{cl}}, M_{\mathrm{pr}}) = -\frac{\partial M_{\mathrm{cl}}}{\partial t} = \frac{\partial M_{\mathrm{pr}}}{\partial t} \propto M_{\mathrm{cl}} M_{\mathrm{pr}} \Phi_{\mathrm{cr}}[\varepsilon(M_{\mathrm{cl}}, M_{\mathrm{pr}})], \tag{4}$$

where Φ denotes similarity terms that scale with the conversion fraction of cloud liquid into rain:

$$\Phi_{\mathrm{cc}}(\varepsilon) = 1 + e_1 \varepsilon^{e_2} \frac{(1-\varepsilon^{e_2})^3}{(1-\varepsilon)^2}, \tag{5}$$

$$\Phi_{\mathrm{cr}}(\varepsilon) = \left(\frac{\varepsilon}{e_3 + \varepsilon}\right)^4, \tag{6}$$

where

$$\varepsilon(M_{\mathrm{cl}}, M_{\mathrm{pr}}) = \frac{M_{\mathrm{pr}}}{M_{\mathrm{cl}} + M_{\mathrm{pr}}}, \tag{7}$$

with parameter values $e_1 = 600$, $e_2 = 0.68$, and $e_3 = 5 \times 10^{-4}$. The dependence of autoconversion on M_{pr} is related to the consideration of spectral broadening (Seifert and Beheng 2001).

b. Mixed and ice phases: Riming, aggregation, and diffusion

Seifert and Beheng describe hydrometeor growth by collection processes involving the ice phase in a uniform way. The mass transfer from a smaller (index s) to a collecting larger hydrometeor (index l) follows

TABLE 2. Integration factors in Eq. (8) based on SB for parameter values in Table 1.

s/l	cl	ci	pr	ps	pg
$\delta_{s,1}$	2.7	3.4	—	—	—
$\theta_{s,1}$	34.	2.7	—	—	—
$\delta_{l,0}$	—	0.8	0.8	0.9	0.9
$\theta_{l,0}$	—	1.5	1.5	1.7	1.3
$\delta_{\mathrm{cl},l,1}$	—	2.3	2.3	2.9	2.7
$\theta_{\mathrm{cl},l,1}$	—	11.	11.	12.	10.
$\delta_{\mathrm{ci},l,1}$	—	2.5	2.6	2.1	2.9
$\theta_{\mathrm{ci},l,1}$	—	3.9	3.7	4.1	3.5

$$\begin{aligned}\mathrm{coll}(M_s,M_l,N_s,N_l) &= -\frac{\partial M_s}{\partial t} = \frac{\partial M_l}{\partial t}\\ &\propto E N_l M_s(\delta_{l,0}D_l^2+\delta_{l,s,1}D_sD_l+\delta_{s,1}D_s^2)\\ &\times(\vartheta_{l,0}v_l^2-\vartheta_{l,s,1}v_sv_l+\vartheta_{s,1}v_s^2+\sigma_s+\sigma_l)^{1/2},\end{aligned} \tag{8}$$

with collection efficiency E, hydrometeor diameters D, and fall velocities v following

$$D_x = a_x(M_xN_x^{-1})^{b_x}, \quad v_x = \alpha_x(M_xN_x^{-1})^{\beta_x} \tag{9}$$

(constants are given in Table 1). The factors δ and ϑ are integration constants depending on the hydrometeor-size distributions (values are given in Table 2).

Collection processes require certain minimum diameters $D_{\mathrm{min},x}$ for collection efficiencies $E > 0$ (Table 3). Graupel–graupel and graupel–ice collision are always assumed unsuccessful. For droplet-riming processes, the collection efficiency E depends on the diameter of the riming droplet:

$$E_{\text{ic-rim}}(D_{\mathrm{cl}}) = \min\left(1, \frac{D_{\mathrm{cl}}-D_{\mathrm{cl,min}}}{D_{\mathrm{cl,max}}-D_{\mathrm{cl,min}}}\right) \tag{10}$$

(constants are given in Table 3).

For aggregation processes (i.e., collection processes between two ice-phase hydrometeors), the collection efficiency is determined by the sticking efficiency and results in a temperature-dependent prefactor that drops out on differentiation.

Growth or evaporation of hydrometeors by diffusion of water vapor onto or from the hydrometeor population is determined by

$$\begin{aligned}x\text{-diff}(M_x,N_x) &= \pm\frac{\partial M_x}{\partial t} \propto N_xD_xF(v_x,D_x)\\ &= N_xD_x(d_1+d_2\sqrt{v_xD_x}),\end{aligned} \tag{11}$$

where F is a ventilation coefficient. (The values of the constants are summarized in Table 4.) The current implementation of the SB scheme in COSMO handles condensation and evaporation of droplets independent of droplet size by means of a saturation adjustment. Only diffusional growth of ice-phase hydrometeors and evaporation of drops below cloud base are described using Eq. (11). The WBF process accordingly only depends on the size of the ice-phase hydrometeors, not on droplet size. To capture the full sensitivity of the WBF process, we will apply Eq. (11) to describe evaporation of droplets in the following.

3. Analytical discussion of partial precipitation susceptibilities

For vanishing divergence of precipitation hydrometeor fluxes, the contribution of a cloudy volume of air to the column precipitation rate P equals the production of precipitation PP in the volume: $\partial P/\partial z = \mathrm{PP}$. Interchanging integration and derivative results in

$$\begin{aligned}\frac{\partial \ln P}{\partial \ln N_x} &= \frac{1}{P}\frac{\partial P}{\partial \ln N_x} = \frac{1}{P}\frac{\partial\left(\int \mathrm{PP}\,dz\right)}{\partial \ln N_x}\\ &= \frac{1}{P}\int\frac{\partial \mathrm{PP}}{\partial \ln N_x}dz = \frac{1}{P}\int\frac{\partial \ln \mathrm{PP}}{\partial \ln N_x}\mathrm{PP}\,dz\end{aligned} \tag{12}$$

such that precipitation susceptibility is the column average of precipitation production susceptibility, weighted with precipitation production. Precipitation susceptibility can thus be approximated by the susceptibility of precipitation production in those regions of a cloud that contribute most to overall precipitation.

In the microphysics scheme, PP corresponds to the transfer of condensate from the crystal (ci) and droplet (cl) hydrometeor class to the larger hydrometeor classes (pr,

TABLE 3. Critical (equivalent) diameter (μm) for collection processes. Water droplets smaller than $D_{\mathrm{min,pr}}$ do not belong to the rain but to the cloud droplet category. Values marked with an asterisk follow the current implementation of the scheme in the COSMO model and differ from SB.

cl + ci	cl + ps	cl + pg	ci + ci	ci + pr
$D_{\mathrm{min,cl}} = 10^*$	$D_{\mathrm{min,cl}} = 10^*$	$D_{\mathrm{min,cl}} = 10^*$	$D_{\mathrm{min,ci}} = 50$	$D_{\mathrm{min,ci}} = 100$
$D_{\mathrm{max,cl}} = 40$	$D_{\mathrm{max,cl}} = 40$	$D_{\mathrm{max,cl}} = 40$		
$D_{\mathrm{min,ci}} = 150$	$D_{\mathrm{min,ps}} = 150$	$D_{\mathrm{min,pg}} = 100^*$		$D_{\mathrm{min,pr}} = 80$

TABLE 4. Coefficients in Eq. (11) based on SB for values from Table 1 and updated ventilation parameters $a_v = 0.78$ and $b_v = 0.308$ (Noppel et al. 2010).

Hydrometeor	d_1	d_2
cl	0.598	62.0
ci	0.589	57.0
ps	0.494	52.4
pg	0.676	61.8
pr	0.598	55.3

ps, and pg), which are large enough to exhibit significant fall velocities. Precipitation is produced by autoconversion (aut), accretion (acc), riming (rim), aggregation (agg), and positive net vapor deposition (diff) on rain and ice-phase hydrometeors and reduced by negative net vapor deposition (i.e., sublimation/evaporation):

$$\mathrm{PP} = \mathrm{aut} + \mathrm{acc} + \mathrm{rim} + \mathrm{agg} \pm \mathrm{diff}. \tag{13}$$

For mixed-phase clouds at or below water saturation, diff stands for the WBF process.

The susceptibility of precipitation production to changes in prognostic moments X of the hydrometeor distributions is the weighted sum of the susceptibilities of the individual processes:

$$\frac{\partial \ln \mathrm{PP}}{\partial \ln X} = \frac{1}{\mathrm{PP}} \frac{\partial \mathrm{PP}}{\partial \ln X} = \sum_{r \in R} \frac{r}{\mathrm{PP}} \frac{\partial \ln r}{\partial \ln X}$$
$$R = \{\mathrm{aut}, \mathrm{acc}, \mathrm{rim}, \mathrm{agg}, \mathrm{diff}\}. \tag{14}$$

In the following, we will derive the partial derivatives of Eqs. (3), (4), (8), and (11) as functions of all prognostic moments, that is,

$$\frac{\partial \ln r(M_{\mathrm{cl}}, M_{\mathrm{ci}}, M_{\mathrm{pr}}, M_{\mathrm{ps}}, M_{\mathrm{pg}}, N_{\mathrm{cl}}, N_{\mathrm{ci}}, N_{\mathrm{pr}}, N_{\mathrm{ps}}, N_{\mathrm{pg}})}{\partial \ln X}$$
$$r \in R$$
$$X \in \{M_{\mathrm{cl}}, M_{\mathrm{ci}}, M_{\mathrm{pr}}, M_{\mathrm{ps}}, M_{\mathrm{pg}}, N_{\mathrm{cl}}, N_{\mathrm{ci}}, N_{\mathrm{pr}}, N_{\mathrm{ps}}, N_{\mathrm{pg}}\}. \tag{15}$$

a. Warm-phase precipitation production

As pure power law [Eq. (3)], the susceptibility of autoconversion to droplet number N_{cl} is a constant:

$$\frac{\partial \ln[\mathrm{aut}(M_{\mathrm{cl}}, M_{\mathrm{pr}}, N_{\mathrm{cl}})]}{\partial \ln N_{\mathrm{cl}}} = -2. \tag{16}$$

The contribution of the scaling functions Φ in Eqs. (3) and (4) makes the remaining warm susceptibilities one-dimensional functions of the rain fraction ε:

$$\frac{\partial \ln[\mathrm{aut}(M_{\mathrm{cl}}, M_{\mathrm{pr}}, N_{\mathrm{cl}})]}{\partial \ln M_{\mathrm{cl}}} = 4 - (1-\varepsilon)\frac{\partial \ln \Phi_{\mathrm{cc}}}{\partial \ln \varepsilon}, \tag{17}$$

$$\frac{\partial \ln[\mathrm{aut}(M_{\mathrm{cl}}, M_{\mathrm{pr}}, N_{\mathrm{cl}})]}{\partial \ln M_{\mathrm{pr}}} = (1-\varepsilon)\frac{\partial \ln \Phi_{\mathrm{cc}}}{\partial \ln \varepsilon}, \tag{18}$$

$$\frac{\partial \ln[\mathrm{acc}(M_{\mathrm{cl}}, M_{\mathrm{pr}})]}{\partial \ln M_{\mathrm{cl}}} = 1 - (1-\varepsilon)\frac{\partial \ln \Phi_{\mathrm{cr}}}{\partial \ln \varepsilon}, \tag{19}$$

$$\frac{\partial \ln[\mathrm{acc}(M_{\mathrm{cl}}, M_{\mathrm{pr}})]}{\partial \ln M_{\mathrm{pr}}} = 1 + (1-\varepsilon)\frac{\partial \ln \Phi_{\mathrm{cr}}}{\partial \ln \varepsilon}, \tag{20}$$

with

$$\frac{\partial \ln \Phi_{\mathrm{cc}}}{\partial \ln \varepsilon} = \frac{e_1 \varepsilon^{e_2}}{(1-\varepsilon)} \cdot \frac{(\varepsilon^{e_2}-1)^2[e_2(\varepsilon-1)(4\varepsilon^{e_2}-1) - 2\varepsilon(\varepsilon^{e_2}-1)]}{1 - 2\varepsilon + \varepsilon^2 - 3e_1\varepsilon^{2e_2} + 3e_1\varepsilon^{3e_2} - e_1\varepsilon^{4e_2} + e_1\varepsilon^{e_2}} \tag{21}$$

and

$$\frac{\partial \ln \Phi_{\mathrm{cr}}}{\partial \ln \varepsilon} = \frac{4e_3}{\varepsilon + e_3}. \tag{22}$$

The susceptibility functions are illustrated in Fig. 2. While the susceptibilities of accretion are effectively determined by the linear factors, autoconversion susceptibility differs by about ± 1 from the exponents of the power-law factors. This especially leads to a significant susceptibility of autoconversion to rain water content and keeps the susceptibility $\partial \ln(\mathrm{aut})/\partial \ln M_{\mathrm{cl}}$ strong in comparison to other schemes (Wood 2005).

b. Precipitation production by riming and aggregation

Riming and aggregation rates are four-dimensional functions of the masses and numbers of the two interacting hydrometeors. Susceptibilities of these collection processes (coll) are two-dimensional functions, when the average masses

$$x_x = \frac{M_x}{N_x} \tag{23}$$

are chosen as variables. This becomes apparent when eliminating the direct mass dependency (or alternatively the direct number dependency) of Eq. (8) with the average mass

$$\mathrm{coll} \propto E M_s M_l \frac{f(x_s, x_l)}{x_l}, \tag{24}$$

where $E = E(x_{\mathrm{cl}})$ for riming with cloud droplets [Eq. (10)] and $E = 1$ otherwise. The geometric part of the collection kernel follows:

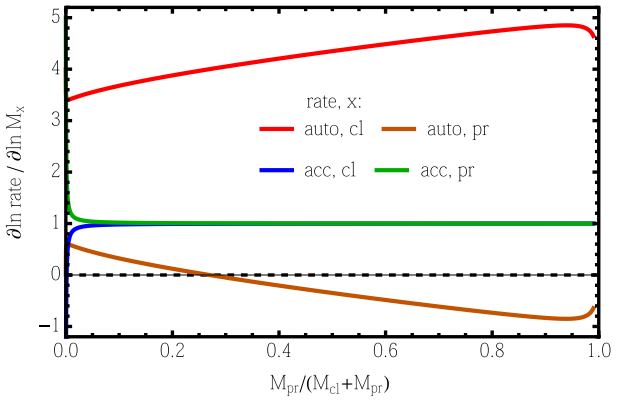

FIG. 2. Mass susceptibilities of autoconversion and accretion rate as a function of rain fraction.

$$\begin{aligned} f(x_s, x_l) &= (\delta_{l,0} a_l^2 x_l^{2b_l} + \delta_{l,s,1} a_s a_l x_s^{b_s} x_l^{b_l} + \delta_{s,1} a_s^2 x_s^{2b_s}) \\ &\times (\vartheta_{l,0} \alpha_l^2 x_l^{2\beta_l} - \vartheta_{l,s,1} \alpha_s \alpha_l x_s^{\beta_s} x_l^{\beta_l} \\ &+ \vartheta_{s,1} \alpha_s^2 x_s^{2\beta_s} + \sigma_s + \sigma_l)^{1/2} \\ &=: f_D(x_s, x_l) \times f_v^{1/2}(x_s, x_l), \end{aligned} \tag{25}$$

where f_D refers to the diameter-dependent part of the collection kernel and f_v to the velocity term.

As constant prefactors drop out in logarithmic differentiation, applying the chain rule results in the following susceptibilities:

$$\begin{aligned} &\frac{\partial \ln[\mathrm{coll}(M_s, M_l, N_s, N_l)]}{\partial \ln N_s} \\ &= \frac{\partial \ln x_s}{\partial \ln N_s} \times \frac{\partial \ln[E f(x_s, x_l)/x_l]}{\partial \ln x_s} \\ &= -\frac{\partial \ln[E f(x_s, x_l)]}{\partial \ln x_s}, \end{aligned} \tag{26}$$

$$\begin{aligned} &\frac{\partial \ln[\mathrm{coll}(M_s, M_l, N_s, N_l)]}{\partial \ln M_s} \\ &= \frac{\partial \ln M_s}{\partial \ln M_s} + \frac{\partial \ln x_s}{\partial \ln M_s} \times \frac{\partial \ln[E f(x_s, x_l)/x_l]}{\partial \ln x_s} \\ &= 1 + \frac{\partial \ln[E f(x_s, x_l)]}{\partial \ln x_s}, \end{aligned} \tag{27}$$

$$\begin{aligned} &\frac{\partial \ln[\mathrm{coll}(M_s, M_l, N_s, N_l)]}{\partial \ln N_l} \\ &= \frac{\partial \ln x_l}{\partial \ln N_l} \times \frac{\partial \ln[E f(x_s, x_l)/x_l]}{\partial \ln x_l} \\ &= 1 - \frac{\partial \ln[E f(x_s, x_l)]}{\partial \ln x_l}, \quad \text{and} \end{aligned} \tag{28}$$

$$\begin{aligned} &\frac{\partial \ln[\mathrm{coll}(M_s, M_l, N_s, N_l)]}{\partial \ln M_l} \\ &= \frac{\partial \ln M_l}{\partial \ln M_l} + \frac{\partial \ln x_l}{\partial \ln M_l} \cdot \frac{\partial \ln[E f(x_s, x_l)/x_l]}{\partial \ln x_l} \\ &= \frac{\partial \ln[E f(x_s, x_l)]}{\partial \ln x_l}. \end{aligned} \tag{29}$$

Summands on the right-hand sides of Eqs. (27) and (28) that amount to 1 represent the effect of an increasing amount of collected mass with increasing small-hydrometeor mass and the effect of an increasing number of collisions with increasing number of large hydrometeors. These effects are modified by the derivatives of the collection kernel $E \times f$. The susceptibility to changes in small-hydrometeor number corresponds to the negative of the susceptibility of the collection kernel to small-hydrometeor size because f only depends on hydrometeor sizes. Likewise, the susceptibility to changes in large hydrometeor mass is given by the susceptibility of the collection kernel to large hydrometeor size. As a consequence, susceptibilities with respect to mass and number of the same hydrometeor category add up to one.

As an example, we give the expression for the susceptibility of the collection kernel for ice–droplet riming to droplet number:

$$\begin{aligned} &\frac{\partial \ln[E(x_{\mathrm{cl}}) f(x_{\mathrm{cl}}, x_{\mathrm{ci}})]}{\partial \ln x_{\mathrm{cl}}} \\ &= \frac{a_c b_c x_c^{b_c} (\delta_{i,c,1} a_i x_i^{b_i} + 2\delta_{s,1} a_c x_c^{b_c})}{f_R(x_c, x_i)} \\ &+ \frac{\alpha_c \beta_c x_c^{\beta_c} (2\vartheta_{c,1} \alpha_c x_c^{\beta_c} - \vartheta_{i,c,1} \alpha_i x_i^{\beta_i})}{2 f_v(x_c, x_i)} \\ &+ \begin{cases} \dfrac{a_{\mathrm{cl}} b_{\mathrm{cl}} x_{\mathrm{cl}}^{b_{\mathrm{cl}}}}{a_{\mathrm{cl}} x_{\mathrm{cl}}^{b_{\mathrm{cl}}} - D_{\mathrm{cl,min}}} & \text{if} \quad a_{\mathrm{cl}} x_{\mathrm{cl}}^{b_{\mathrm{cl}}} \le D_{\mathrm{cl,max}} \\ 0 & \text{otherwise} \end{cases}. \end{aligned} \tag{30}$$

Susceptibilities with respect to other moments are very similar to this expression. They can be derived when taking into account that Eq. (25) depends on x_s and x_l in a structurally symmetric way in the sense that both variables can be exchanged when exchanging prefactors and exponents accordingly. The last term with the distinction of cases is only present for cloud-riming processes.

As susceptibilities with respect to mass and number of the same hydrometeor category add up to one, we restrict visualization of susceptibilities in Figs. 3 and 4

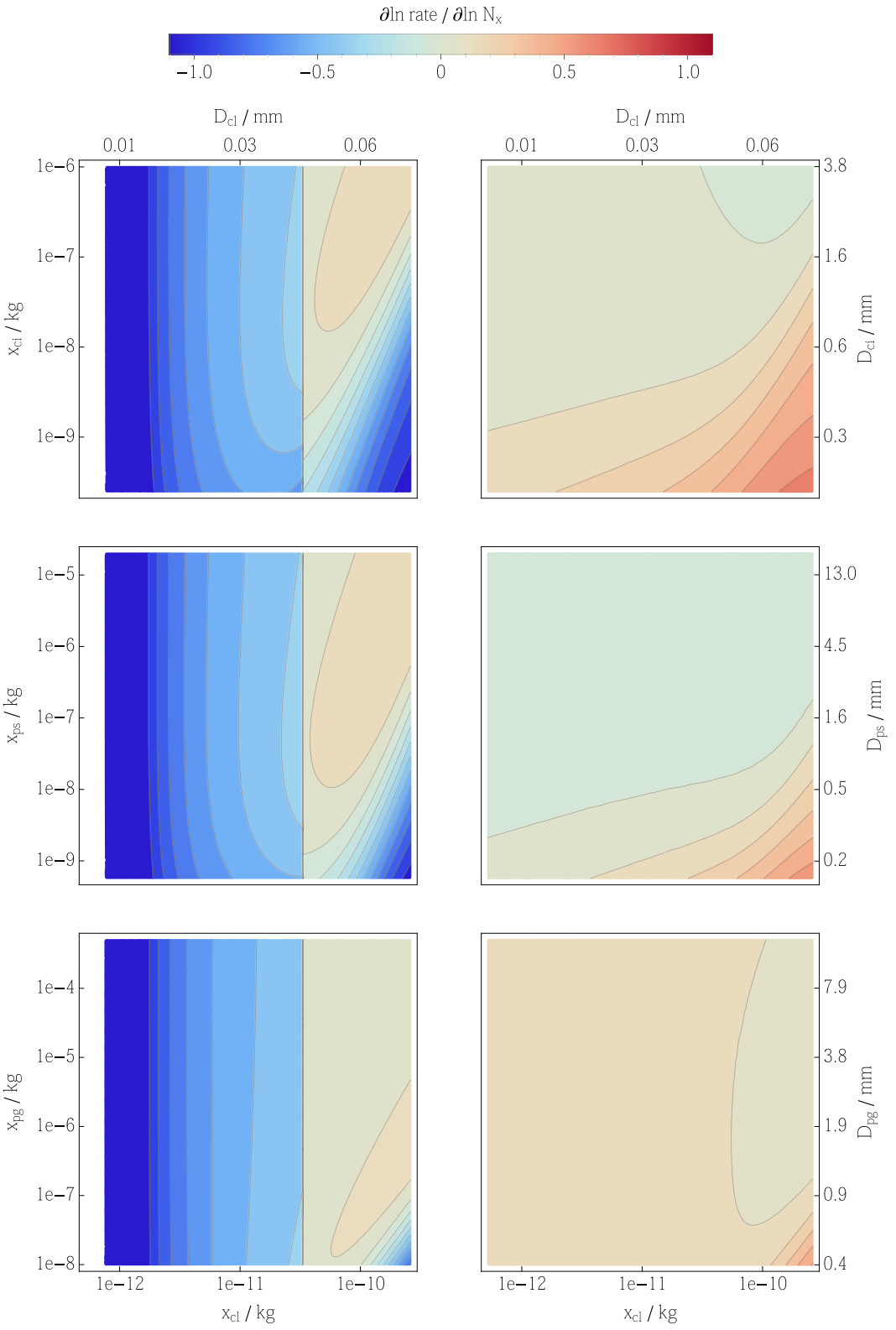

FIG. 3. Susceptibilities of (top) ice-droplet riming, (middle) snow-droplet riming, and (bottom) graupel-droplet riming to changes in (left) collected ($N_x = N_s$) and (right) collecting ($N_x = N_l$) hydrometeor numbers as a function of average hydrometeor masses and diameters, respectively. Axes ranges reflect minimal and maximal values defining the hydrometeor class and the onset of riming according to Table 3.

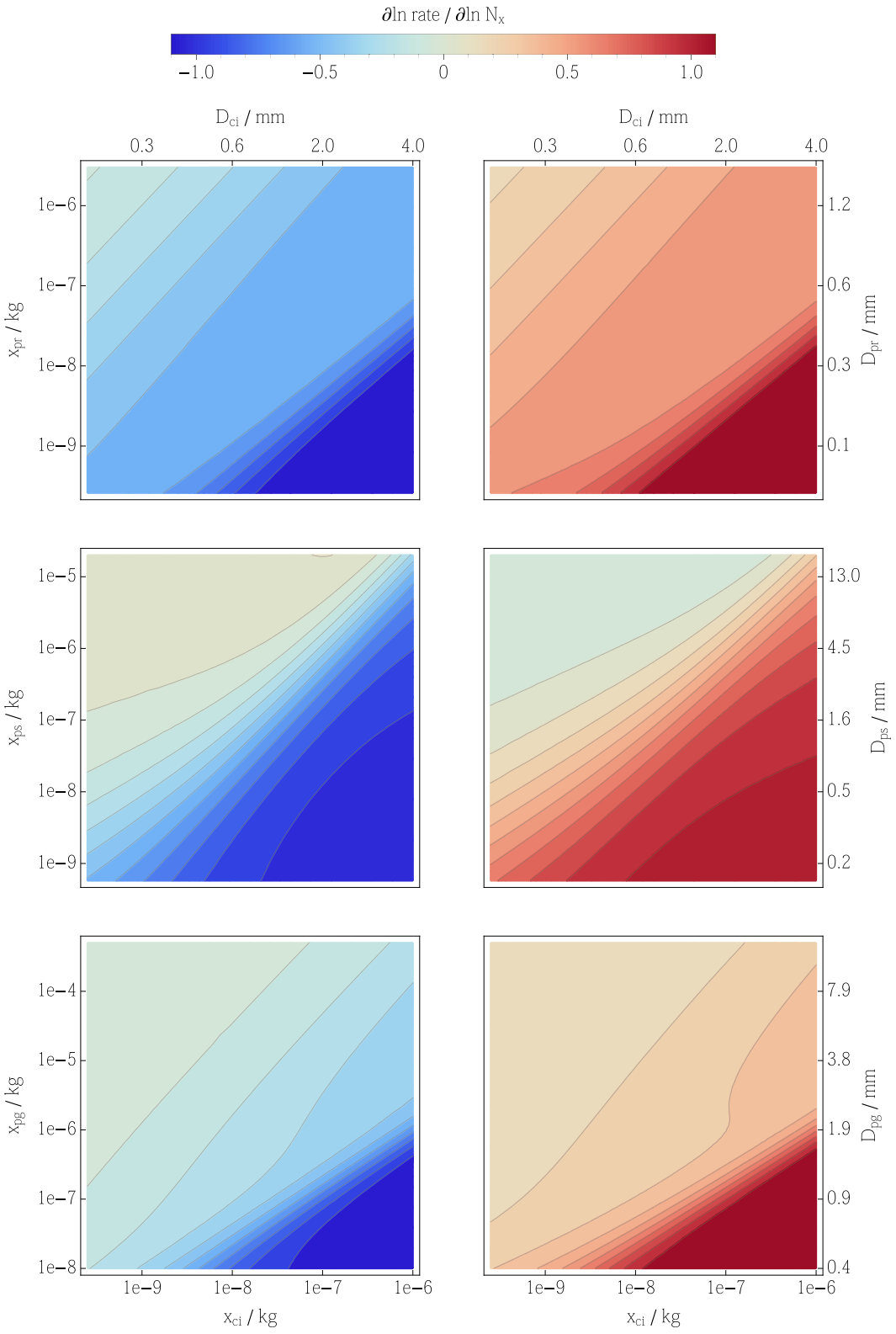

FIG. 4. Susceptibilities of (top) ice-rain riming, (middle) snow–ice aggregation, and (bottom) graupel–ice aggregation to changes in (left) collected ($N_x = N_s$) and (right) collecting ($N_x = N_l$) hydrometeor numbers as a function of average hydrometeor masses and diameters, respectively. Axes ranges reflect minimal and maximal values defining the hydrometeor class and the onset of riming according to Table 3.

to number susceptibilities. Susceptibilities of riming processes to droplet number (Fig. 3, left column) are dominated by the susceptibility of the collection efficiency term with values from −0.5 to −2.5. For droplet sizes $a_{cl}x_{cl}^{b_{cl}} > D_{max,cl}$, or $x_{cl} > 3 \times 10^{-11}$ kg, respectively, the collection efficiency takes a constant value of unity such that its contribution to the susceptibility abruptly vanishes. Apart from this contribution, number susceptibilities of riming processes with droplets tend to be smaller than 0.2 in magnitude. Susceptibilities of collection processes with precipitation-sized hydrometeors to crystal number (Fig. 4, left column) exhibit values from around 0 to 1.

Excluding the collection efficiency contribution, susceptibilities to changes in crystal number are negative, while those to droplet number tend to be positive. This difference is a consequence of droplet aerodynamic properties in combination with the basic structure of the geometric part of the collection kernel:

$$f \approx (v_l - v_s) \times (D_l + D_s)^2 \sim \begin{cases} -x_s^{\beta_s} + x_s^{2/3} & \text{for} \quad x_l = \text{const} \\ x_l^{2/3+1/5} & \text{for} \quad x_s = \text{const} \end{cases}, \tag{31}$$

where the exponent of the diameter–mass relationship can be approximated by $b_x \approx 1/3$ for all hydrometeor classes and the exponent of the fall velocity–mass relationship by $\beta_l = 1/5$ for collecting ice-phase hydrometeors (cf. Table 1 for exact values). The collection kernel on the one hand tends to increase with increasing diameters of the colliding particles and thus an increased cross section for the collision. This causes positive susceptibilities with respect to size and negative susceptibility with respect to number. On the other hand, the collection kernel decreases with decreasing relative fall speed of the collision partners, an effect that corresponds to negative susceptibility to the size and positive susceptibility to the number of the collected hydrometeor. For collecting hydrometeors, cross section and fall speed are increased by increasing size, which leads to strictly positive susceptibilities with respect to size and strictly negative susceptibilities with respect to numbers.

For the dependence of ice-droplet riming on droplet size, we have $\beta_s = 2/3$ in Eq. (31) such that both terms are comparable and the negative term can determine the sign. The minus sign is not a general prefactor and does not cancel in the logarithmic derivative. For ice as collected particle, we have $\beta_s = 1/5$ (Table 1) such that the positive diameter term is always expected to dominate. An increase in droplet number thus increases riming efficiency at fixed M_{cl} because droplet fall speed is very sensitive to droplet size such that the increasing effect of decreasing droplet size on the difference in fall speed dominates over the decreasing effect on cross section. An increase in crystal number decreases the efficiencies of ice–rain riming and aggregation of ice by snow and graupel because crystal fall speed is comparably insensitive to crystal size such that the effect on cross section dominates over the effect on fall speed difference. Dominance of the velocity versus diameter term in the collection kernel also explains the differently shaped contours in Fig. 3 as compared to Fig. 4: The diameter term results in diagonal contours, while the velocity term features an elliptical structure.

Susceptibilities to changes in the number of collecting hydrometeors (Figs. 3, 4, right columns) are a combination of the positive contribution from an increase in the number of collisions [unity term in Eq. (28)] and an inhibiting effect of number on hydrometeor size (at constant mass) via the collection kernel, as discussed in the context of Eq. (31). The latter effect is especially pronounced for ice-droplet and snow-droplet riming (and to a slightly lesser extent graupel-droplet riming), where it leads to compensation and susceptibilities close to zero. As the sum of mass and number susceptibilities equals 1, these low susceptibilities with respect to number correspond to strong susceptibilities around 1 to the average mass of ice and snow particles. This is consistent with the fractal shape of these hydrometeors leading to a pronounced increase of size and collisional cross section per mass increase.

Mass susceptibilities are positive, as number susceptibilities typically do not take values < -1 and mass and number susceptibilities sum up to 1. This is to be expected from Eqs. (27) and (29), as susceptibilities of the geometric part of the collection kernel to hydrometeor size can only be negative for cloud droplets, as discussed in the context of Eq. (31). Because of compensating effects on fall speed and cross-sectional term, no strongly negative values are possible, however.

c. *Precipitation production by self-collection of ice crystals*

Ice–ice self-collection $\text{self}(M_{ci}, N_{ci}) = \text{coll}(M_{ci}, M_{ci}, N_{ci}, N_{ci})$ depends quadratically on crystal mass because the latter affects both collision partners at the same time. This quadratic dependence results in susceptibilities structurally different from aggregation processes between hydrometeors of different size:

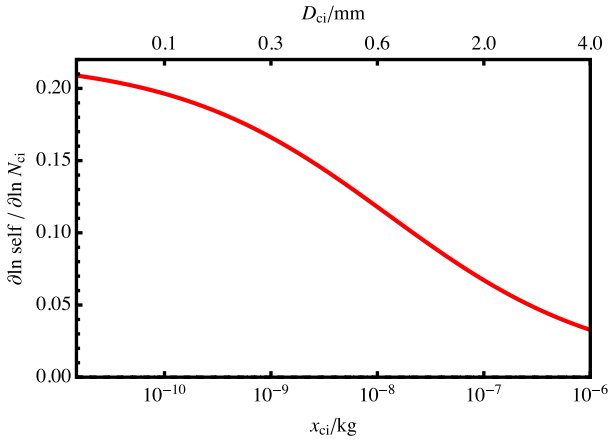

FIG. 5. Susceptibility of ice self-collection as a function of average ice crystal mass or diameter.

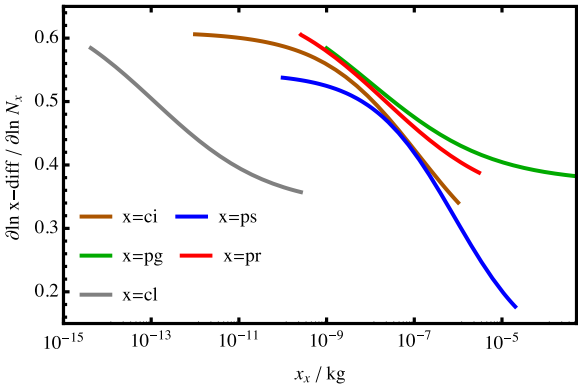

FIG. 6. Susceptibility of hydrometeor–vapor exchange with respect to numbers as a function of average hydrometeor mass. Susceptibilities are only plotted in the defining size range of each hydrometeor class in SB.

$$\frac{\partial \ln[\mathrm{self}(M_{ci},N_{ci})]}{\partial \ln N_{ci}} = \frac{\partial \ln x_{ci}}{\partial \ln N_{ci}} \cdot \frac{\partial \ln[f(x_{ci})/x_{ci}]}{\partial \ln x_{ci}} = 1 - \frac{\partial \ln f(x_{ci})}{\partial \ln x_{ci}} \tag{32}$$

$$\frac{\partial \ln[\mathrm{self}(M_{ci},N_{ci})]}{\partial \ln M_{ci}} = \frac{\partial \ln M_{ci}^2}{\partial \ln M_{ci}} + \frac{\partial \ln x_{ci}}{\partial \ln M_{ci}} \cdot \frac{\partial \ln[f(x_{ci})/x_{ci}]}{\partial \ln x_{ci}} = 1 + \frac{\partial \ln f(x_{ci})}{\partial \ln x_{ci}} \tag{33}$$

where mass and number susceptibilities add up to 2. The derivative with respect to average mass reads as follows:

$$\frac{\partial \ln f(x_{ci})}{\partial \ln x_{ci}} = 2b_{ci} + \beta_{ci}\left[1 - \frac{2\sigma_{ci}}{f_v(x_{ci},x_{ci})}\right]. \tag{34}$$

Number susceptibilities are smaller than 0.2 and correspond to mass susceptibilities larger than one (Fig. 5). The number susceptibility decreases with increasing crystal size. This corresponds to an increase of the susceptibility of the collection kernel caused by a decreased compensating effect of the relative fall velocity term. This term becomes irrelevant as crystal fall speeds grow large compared to the velocity variance term σ_{ci}, which is the only source for differences in relative fall speed for self-collection.

d. *Contribution of vapor diffusion to precipitation production*

Similar to the collection processes, susceptibilities of vapor deposition, evaporation, and sublimation only depend on average masses. Equation (11) can be rewritten as

$$x - \mathrm{diff} \propto N_x D_x(x_x) F(x_x) \tag{35}$$

such that the logarithmic derivative follows

$$\frac{\partial \ln[x - \mathrm{diff}(M_x,N_x)]}{\partial \ln N_x} = 1 - b_x - \frac{\partial \ln F(x_x)}{\partial \ln x_x} \quad \text{and} \tag{36}$$

$$\frac{\partial \ln[x - \mathrm{diff}(M_x,N_x)]}{\partial \ln M_x} = b_x + \frac{\partial \ln F(x_x)}{\partial \ln x_x}, \tag{37}$$

with mass and number susceptibilities adding up to one. The derivative of the ventilation coefficient reads

$$\frac{\partial \ln F(x_x)}{\partial \ln x_x} = \frac{b_x + \beta_x}{2}\left[1 - \frac{d_1}{F(x_x)}\right] \tag{38}$$

and causes a decrease in number susceptibility as the diameter-dependent term of the ventilation coefficient gains importance (Fig. 6). Reflecting the dependence of diffusional efficiency on hydrometeor surface, susceptibilities remain positive. Their intermediate values range from 0.35 to 0.6 for droplets, crystals, graupel, and rain and from 0.2 to 0.5 for snowflakes.

In mixed-phase clouds at or below water-saturated conditions, combining the susceptibility of evaporation of droplets and diffusional growth of ice-phase hydrometeors gives the susceptibility of the WBF process. For simulations with a saturation adjustment, the WBF process is not susceptible to droplet number or mass.

e. *Comparison of process susceptibilities*

To simplify the following discussion, Table 5 summarizes each partial susceptibility function, or susceptibility

TABLE 5. Typical susceptibility values of precipitation formation processes. Dashes indicate nonsusceptibility.

Rate	$\frac{\partial \ln(\text{Rate})}{\partial \ln N_s}$	$\frac{\partial \ln(\text{Rate})}{\partial \ln M_s}$	$\frac{\partial \ln(\text{Rate})}{\partial \ln N_l}$	$\frac{\partial \ln(\text{Rate})}{\partial \ln M_l}$
aut	−2.0	4.3	—	−0.3
acc	—	1.0	—	1.0
ic-rim	−0.5	1.5	—	1.0
sc-rim	−0.5	1.5	—	1.0
gc-rim	−0.5	1.5	0.1	0.9
self	0.1	1.9	—	—
ir-rim	−0.5	1.5	0.5	0.5
is-agg	−0.3	1.3	0.4	0.6
ig-agg	−0.2	1.2	0.2	0.8
cl-diff	0.4	0.6	—	—
ci-diff	0.6	0.4	—	—
ps-diff	—	—	0.4	0.6
pg-diff	—	—	0.4	0.6
pr-diff	—	—	0.5	0.5
WBF	0.4	0.6	0.5	0.5

plot, respectively, by a single typical value. This means that we restrict the discussion to a certain range of cloud states corresponding to susceptibility values represented by the typical value. As discussed in the context of Eq. (1), values may be interpreted as typical percentage change in the respective rate that results from a 1% change in M or N, respectively. We use susceptibility values obtained from evaluating the susceptibility functions in the center of the plots, that is, at $\log_{10}x = 0.5[\log_{10}(x_{\min}) + \log_{10}(x_{\max})]$ and $\varepsilon = 0.5$, where $[x_{\min}, x_{\max}]$ denotes the definition range. Some kind of average would, in principle, be preferable but requires distributions of typical hydrometeor sizes, which especially for the ice phase are not readily available. Taking central values instead provides a reasonable approximation: Hydrometeor sizes close to the boundaries of the domain of definition are less likely to be encountered in a generic cloud than values in the center of the domain. Additionally, this approach avoids extreme susceptibility values that occur when hydrometeor sizes approach their boundary values $x_{\min}$ and $x_{\max}$.

The first column of Table 5 shows that autoconversion, riming, and aggregation are less efficient in producing precipitation for more but smaller droplets or crystals. The efficiencies of diffusional growth and, to a lesser extent, self-collection are instead increased. Increasing hydrometeor size at constant numbers increases precipitation formation for all processes except autoconversion (columns 2 and 4 of Table 5). At low values of ε, for which autoconversion dominates over accretion, autoconversion follows the general trend of intensified precipitation formation from larger hydrometeors (Fig. 2). Increasing the number of large hydrometeors likewise increases efficiency (column 3) for diffusional growth and collection of ice by rain, snow, and graupel. Droplet riming and ice self-collection rates are effectively not influenced by the number of collecting hydrometeors. The difference in susceptibility to the number of collecting hydrometeors between cloud riming and aggregation and ice–rain riming is a result of the combination of parameters in Eq. (8) and cannot be associated with a specific process or hydrometeor property. According to the susceptibilities of diffusion, the WBF process increases for increasing numbers and sizes of droplets and ice-phase hydrometeors.

Autoconversion is the most sensitive process. This high sensitivity is a consequence of the autoconversion collision kernel, which SB based on Long and Manton (1974), as compared to the ice- and mixed-phase collision kernel Eq. (31): The latter scales with the square of hydrometeor radii, whereas the Long kernel scales to the 6th power for the smallest droplets. While a 10% increase in droplet number reduces autoconversion by 20%, riming decreases by 5%, and aggregation would decrease only by 2%–3% as a result of a 10% increase in crystal number. An increase in droplet mass of about 10% leads to a 40% increase in autoconversion rate, but only to a 15% increase in riming. Aggregation is increased by almost 15% for a 10% increase in cloud ice mass.

Susceptibilities for riming and aggregation are overall comparable, whereas ice–graupel and ice–snow aggregation tend to be slightly less susceptible. While riming susceptibility to droplet number is dominated by the collection efficiency, the susceptibility of ice collection by rain, snow, and graupel emerges from the geometric part of the collection kernel.

While vapor diffusion is equally susceptible to mass and number at intermediate positive values, pair-interaction rates are less susceptible to the number of a hydrometeor type than to its mass. The latter indicates that adjustments of hydrometeor masses to changes in numbers may significantly influence precipitation susceptibilities.

f. *Robustness and importance of adjustments*

In the previous sections, partial susceptibilities have been discussed. According to Eq. (1), total precipitation susceptibility requires taking into account the effects of adjustments $d\ln M_{\text{cl}}/d\ln N_{\text{cl}}$ and their cold-phase analogs. Determining adjustments requires the full complexity of cloud processes, including dynamics, thermodynamics, and radiation and is hardly accessible analytically. We investigate instead which adjustment

value corresponds to complete compensation of the partial precipitation susceptibility and leads to a vanishing total susceptibility s. Assuming $\partial \ln P/\partial \ln N_{\rm cl} = -2$ and $\partial \ln P/\partial \ln M_{\rm cl} = 4$, a compensating adjustment of $(d\ln M_{\rm cl}/d\ln N_{\rm cl})_{\rm comp} = 0.5$ leads to $s = 0$ for the example of Eq. (1).

We apply the sketched concept of compensating adjustments to the partial susceptibilities of precipitation production rate r to X. Compensation by adjustments in a hydrometeor moment Y are then given by the following:

$$0 \overset{!}{=} \frac{d\ln r}{d\ln X} = \frac{\partial \ln r}{\partial \ln X} + \frac{\partial \ln r}{\partial \ln Y}\frac{d\ln Y}{d\ln X}\bigg|_{\rm comp}$$
$$\Rightarrow \frac{d\ln Y}{d\ln X}\bigg|_{\rm comp} = -\frac{\partial \ln r}{\partial \ln X}\bigg/\frac{\partial \ln r}{\partial \ln Y}. \qquad (39)$$

The value of a compensating adjustment thus compares the susceptibilities of the process to the correlated variables X and Y. For $|(d\ln Y/d\ln X)_{\rm comp}| \geq 2$ we consider the partial susceptibility $\partial \ln r/\partial \ln X$, or the signal that changes in X cause in r, as robust to adjustments in Y, because the percentage change in Y needs to have twice the strength of the percentage change in X. For $|(d\ln Y/d\ln X)_{\rm comp}| \leq 0.5$ we consider a partial susceptibility as sensitive because compensating adjustments only require half of the strength of the original perturbation.

Table 6 evaluates Eq. (39) for the robustness of crystal and droplet number susceptibilities to adjustments in droplet and crystal mass (left column) and to adjustments in mass and number of precipitation-sized hydrometeors (middle and right columns). Along the lines of Stevens and Feingold (2009), we will denote the latter as feedbacks because the adjusting variable (precipitation-sized hydrometeors) corresponds to the adjusted variable (precipitation production). In most cases, susceptibilities are not robust. Droplet and crystal number susceptibilities tend to be less robust against compensations from their own masses than against feedbacks from precipitation-sized hydrometeors: For the example of ice–snow aggregation (is-agg), a 10% change in crystal number is compensated for in its effect on precipitation production by a 3% change in ice water content, while an 8% change in snow crystal number or a 6% change in snow water content would be required. The susceptibilities of autoconversion and graupel-droplet riming are exceptionally robust to feedbacks in rainwater amount and graupel number, respectively. Both are related to small susceptibilities in the denominator.

TABLE 6. Compensating adjustments to changes in small-hydrometeor number according to Eq. (39) based on the susceptibility values in Table 5. Dashes indicate cases for which no compensating adjustments can be defined because of nonsusceptibility.

Rate	$\frac{d\ln M_s}{d\ln N_s}$	$\frac{d\ln N_l}{d\ln N_s}$	$\frac{d\ln M_l}{d\ln N_s}$
aut	0.5	—	−5.7
ic-rim	0.3	—	0.5
sc-rim	0.3	—	0.4
gc-rim	0.3	4.7	0.6
self	−0.1	—	—
ir-rim	0.4	1.0	1.2
is-agg	0.3	0.8	0.6
ig-agg	0.2	0.9	0.3
ci-diff	−1.3	—	—
WBF	−0.7	−0.9	−0.9

1) ADJUSTMENTS IN CLOUD LIQUID AND ICE CONTENT

For purely microphysical adjustments, the sign of $d\ln M_s/d\ln N_s$ is constrained by cloud microphysical rates: Negative susceptibilities of collection processes to N_s in Table 5 correspond to positive correlations between $d\ln M_s$ and $d\ln N_s$ because an increase in N_s suppresses the corresponding process and thus causes an accumulation of M_s. The positive susceptibilities of diffusional growth in Table 5 introduce a negative correlation for index s = cl because the WBF process depletes cloud water and a positive correlation for s = ci because diffusional growth is a source of cloud ice. For s = cl, susceptibilities of collection processes are larger than that of diffusional growth, while the susceptibility of diffusional growth dominates for s = ci. Based on this observation, we assume positive correlations for both cases.

For $d\ln M_s/d\ln N_s > 0$, we conclude based on Table 6 that compensating adjustments will likely occur for autoconversion, riming, and aggregation because these processes feature positive compensating adjustments. With negative compensating adjustments, ice self-collection, diffusional growth, and the WBF process are instead enhanced by adjustments. For the cold phase, mass and number susceptibilities of the same hydrometeor class add up to one [two for self-collection (cf. sections 3b–3d)] because the collection kernel only is a function of hydrometeor sizes. Cold susceptibilities are thus either weak and positive for mass and number—vapor diffusion and the WBF process being an example—or they have opposite signs allowing for compensating adjustments, as discussed for collection processes.

2) PRECIPITATION FEEDBACK

Adjustments in the number of precipitation-sized hydrometeors do not modify the effect of droplet number on autoconversion and droplet riming (Table 6, middle column). Assuming that the droplet number is not strongly correlated to the number of ice-phase hydrometeors, $d\ln N_{ci/ps/pg}/d\ln N_{cl} \approx 0$ and thus excluding adjustments to the WBF process, susceptibilities with respect to droplet number are not modified by adjustments in the number of precipitation hydrometeors. Susceptibilities with respect to crystal number are ambiguously modified by precipitation number adjustments: Assuming that crystal number is positively correlated with the number of snow and graupel particles, precipitation number adjustments compensate the reducing effect of increasing crystal number on aggregation and enhance its effect on diffusion and the WBF process.

Feedbacks from precipitation amount, $d\ln M_l/d\ln N_s$ with l = pr, ps, pg and s = cl, ci, correspond to total precipitation susceptibility. Negative (positive) precipitation susceptibility corresponds in sign to an enhancing adjustment, that is, a positive, noncompensating feedback, to collection processes (diffusion and the WBF process), which contribute to negative (positive) precipitation susceptibility (Table 6, right column). The precipitation feedback is thus positive and results in more negative (positive) susceptibilities.

This result is based on positive net-diffusional growth and thus is restricted to cloud-base precipitation. For surface precipitation, inverse effects from sublimation of snow and graupel and evaporation of raindrops and melting snow and graupel below cloud base have to be considered. In the following, we try to estimate whether the positive or negative effect of diffusional growth dominates: During their travel from the cloud, where vapor deposition takes place, to below cloud base, where sublimation and evaporation starts, precipitation particles grow in size and reduce in number by pair interactions. We assume that growth by collection of smaller hydrometeors dominates over occasional mutual collection. Precipitation particles will thus be bigger and slightly reduced in number below the cloud as compared to inside the cloud. In addition, the ventilation effect of turbulence is more effective in the subsaturated environment below cloud base. The negative effect of vapor diffusion is thus expected to dominate. Vapor diffusion, in conclusion, poses a positive feedback for cloud-base precipitation and a negative feedback for surface precipitation. The negative effect will be especially important for the slow sedimentation of snow, which increases exposition to sublimation.

3) PERTURBATIONS OF GLACIATION STATE AND RAIN FRACTION

As microphysical rates are generally more affected by mass than by number changes, we investigate the interplay of mass adjustments by studying Eq. (39) for situations where both hydrometeor moments X and Y are masses. These may, in particular, lead to changes in rain fraction ε and for mixed-phase clouds in glaciation fraction

$$\gamma = \frac{I}{L+I}, \tag{40}$$

where $I = M_{ci} + M_{ps} + M_{pg}$ and $L = M_{cl} + M_{pr}$. We only discuss the effect of rain and glaciation fraction on microphysical rates, independent of changes in the relative importance of precipitation formation processes. The latter is strongly related to rain and glaciation fraction and could be taken into account by not only discussing derivatives of rates in Eq. (14) but also derivatives of the weighting factors r/PP.

An aerosol-induced shift in rain fraction ε corresponds to anticorrelated changes of $X = M_{cl}$ and $Y = M_{pr}$ in Eq. (39). An aerosol-induced change in glaciation fraction coincides with anticorrelated changes in ice-phase hydrometeor amount, $Y = I$, and cloud liquid amount, $X = L$. We assume that changes in rain and glaciation fraction result from one-to-one conversions $\Delta M_{cl} = -\Delta M_{pr}$ or $\Delta I = -\Delta L$. The compensating adjustment ratio then corresponds to certain rain and glaciation fractions at which a perturbation to the fraction does not affect microphysical conversion rates:

$$\frac{\Delta\ln M_{pr}}{\Delta\ln M_{cl}} \approx -\frac{M_{cl}}{M_{pr}} = -\frac{1-\varepsilon}{\varepsilon}. \tag{41}$$

The same argument applies to the mixed-phase case when one liquid- and one ice-phase hydrometeor category dominates.

The effect of changes in M_{cl} on autoconversion is very robust to adjustments in M_{pr} and cannot be compensated by an anticorrelated adjustment: According to Table 7, a 12% decrease in rainwater would be required to compensate a 1% decrease in cloud water. While the sign of the compensating adjustment depends on the value of ε, robustness extends to all values of ε as the susceptibility of autoconversion to M_{pr} is significantly smaller in magnitude than that to M_{cl} over the whole range of rain fractions (Fig. 2). Adjustments in rain fraction thus hardly influence the susceptibilities of liquid-phase precipitation production and do not, in particular, modulate the effect of adjustments in cloud liquid water.

TABLE 7. Compensating rain and glaciation fraction adjustments according to Eq. (39) based on (first and second columns) the susceptibility values in Table 5 and (last column) corresponding glaciation fraction. Dashes indicate nonapplicability of the respective adjustment or fraction.

Rate	$\frac{d\ln M_{pr}}{d\ln M_{cl}}$	$\frac{d\ln M_{ci/ps/pg}}{d\ln M_{cl/pr}}$	γ
aut	12	—	—
ic-rim	—	−1.6	0.4
sc-rim	—	−1.4	0.4
gc-rim	—	−1.7	0.4
ir-rim	—	−0.3	0.8
WBF	—	−1.1	0.5

In mixed-phase clouds, anticorrelated changes in liquid- and ice-phase cloud water have compensating influences on riming and the WBF process (Table 7). With the exception of ice–rain riming, complete compensation is reached for intermediate glaciation fractions. For low and high glaciation fractions, the minority phase is subject to strong relative changes by a one-to-one conversion and dominates the response: For predominantly liquid clouds, glaciation increases the efficiency of droplet riming and the WBF process. For ice-dominated clouds, additional glaciation inhibits droplet riming and the WBF process. Glaciation exhibits a positive feedback in weakly glaciated clouds and a negative feedback in strongly glaciated clouds, and it proceeds fastest but with a robust rate at intermediate glaciation fractions.

4. Constraining total precipitation and sedimentation susceptibilities

Precipitation susceptibility can be approximated by precipitation production susceptibility in the regions of a cloud that contribute most to overall precipitation [cf. Eq. (12)]. Partial susceptibilities of precipitation production follow from partial susceptibilities of individual rates according to Eq. (14). In the following, we discuss total precipitation susceptibilities based on these relationships and the following assumptions: (i) Precipitation is predominantly produced in a single cloud region of homogeneous composition; (ii) the microphysical composition in this region is, especially in terms of sign, represented by the typical susceptibility values in Table 5; (iii) non-microphysical adjustments are absent such that adjustments follow the discussion in section 3f. Precipitation susceptibilities of convective cloud types, in particular, may be dominated by dynamical, thermodynamical, or radiative adjustments, which are beyond the scope of this article.

For warm clouds, precipitation is produced via autoconversion and accretion, $\mathrm{PP}_{warm} = \mathrm{aut} + \mathrm{acc}$. As accretion is not susceptible to N_{cl}, the partial susceptibility to droplet number only depends on Eq. (16),

$$\frac{d\ln \mathrm{PP}_{warm}}{d\ln N_{cl}} > \frac{\partial \ln \mathrm{PP}_{warm}}{\partial \ln N_{cl}} = -2\frac{\mathrm{aut}}{\mathrm{aut}+\mathrm{acc}}, \qquad (42)$$

and the total susceptibility will result in larger (i.e., less negative) values as a result of compensating adjustments from liquid water content. If the adjustment does not lead to overcompensation, warm rain is thus expected to decrease with increasing droplet number, which is in line with Albrecht (1989). The strength of the susceptibility decreases with the relative importance of autoconversion, as has been discussed, for example, by Sorooshian et al. (2009), Wood et al. (2009), and Sant et al. (2015): If precipitation is primarily produced by accretion, which is independent of droplet number, it does not change with changing droplet number.

For cirrus clouds, we consider sedimentation of crystals as precipitation. Crystals only grow by vapor deposition because residence times in the cloud are too short for self-collection such that $\mathrm{PP}_{ice} = i\text{-diff}$. According to Table 5, the susceptibility of precipitation production to crystal number is expected to be

$$\frac{d\ln \mathrm{PP}_{ice}}{d\ln N_{ci}} > \frac{\partial \ln \mathrm{PP}_{ice}}{\partial \ln N_{ci}} \approx 0.6, \qquad (43)$$

where the total susceptibility is enhanced by adjustments in ice amount. Susceptibility is positive, indicating increased sedimentation for more but smaller crystals. This result is counterintuitive and contrary to the proposed results of cirrus seeding with ice-nucleating particles (Mitchell and Finnegan 2009; Storelvmo and Herger 2014). These studies discuss that switching from homogeneous nucleation of many small solution droplets to heterogeneous nucleation of fewer crystals leads to larger particles with higher sedimentation velocities and thus a faster dissipation of the cloud.

The key to resolving this discrepancy is that in cirrus clouds the effect of adjustments in supersaturation on diffusional growth cannot be neglected: While saturation ratios in mixed-phase clouds are bound to values close to water saturation, ice supersaturation up to 170% is possible in cirrus (Krämer et al. 2009). Following the theoretical considerations on warm precipitation susceptibility in Feingold et al. (2013), cirrus sedimentation susceptibility can be determined without explicitly dealing with adjustments in supersaturation:

With the sedimentation velocity v_{ci} [Eq. (9)] cirrus sedimentation rate is given by

$$P_{ice} = M_{ci} v_{ci} \propto M_{ci} \left(\frac{M_{ci}}{N_{ci}}\right)^{\beta_{ci}} = M_{ci}^{1+\beta_{ci}} N_{ci}^{-\beta_{ci}} \quad (44)$$

such that the partial susceptibilities with respect to crystal number and ice mass are given by −0.2 and 1.2 (cf. Table 1). The corresponding argument for warm, mixed-phase, and ice clouds is impeded because it results in comparing mass and sedimentation velocities of precipitation-size hydrometeors to mass and number of droplets and crystals.

The exact development of supersaturation and thus diffusional growth in cirrus depends on the prevalent ice-nucleation mechanism (Kuebbeler et al. 2014) but tends to eventually reach ice saturation (Krämer et al. 2009). Total diffusional growth is accordingly limited by available supersaturation and can be assumed independent of crystal size. The total sedimenting ice amount M_{ci} is thus independent of microphysics, and precipitation susceptibility is given by the susceptibility of sedimentation velocity:

$$\frac{d\ln P_{ice}}{d\ln N_{ci}} = \frac{d\ln v_{ci}}{d\ln N_{ci}} = -\beta_{ci} \approx -0.2. \quad (45)$$

It is negative, in accordance with theories about cirrus seeding (Mitchell and Finnegan 2009; Storelvmo and Herger 2014). Absolute susceptibility is low: To obtain a 20% increase in sedimentation rate, a 100% decrease in crystal number is required. Whether such a strong decrease in crystal number is realized depends on the fraction of homogeneous freezing that is replaced by heterogeneous freezing. For incomplete replacement, the remaining homogeneous freezing can easily continue to dominate crystal number and lead to small relative changes (Penner et al. 2015).

For mixed-phase clouds, all processes in Eq. (14) are relevant. We only consider changes in vapor diffusion and the WBF process affecting the precipitation-sized hydrometeors snow and graupel (denoted by pWBF) as changes in precipitation formation. Changes in vapor diffusion to crystals are considered as part of adjustments in ice amount. As the WBF process and thus ice amount is enhanced by more and/or larger crystals as well as by more and/or larger droplets (Table 5), adjustments in ice amount modify susceptibilities with respect to droplet and crystal number. A crystal number perturbation additionally triggers positive ice adjustments via ice accumulation from reduced aggregation efficiency and diffusional growth in non-WBF conditions (Table 5). Ice adjustments to crystal number perturbations, $d\ln M_{ci}/d\ln N_{ci}$, are thus expected to be stronger than those to droplet number perturbations, $d\ln M_{ci}/d\ln N_{cl}$. We refer to these ice adjustments as glaciation adjustments. These are expected to be especially strong at low glaciation fractions, where the WBF process is self-enhancing [cf. section 3f(3)].

With Table 5, the susceptibility of mixed-phase precipitation production to droplet number is approximately

$$\frac{d\ln \mathrm{PP}}{d\ln N_{cl}} > \frac{\partial \ln \mathrm{PP}}{\partial \ln N_{cl}} \approx -2.0\frac{\mathrm{aut}}{\mathrm{PP}} - 0.5\frac{\mathrm{rim}}{\mathrm{PP}} + 0.4\frac{\mathrm{pWBF}}{\mathrm{PP}}, \quad (46)$$

where we have combined all droplet–riming processes in rim, using their average susceptibility. The effect of liquid adjustments parallels that in warm clouds by shifting all three terms on the right-hand side to less negative or more positive values, respectively. The primary effect of a glaciation adjustment is to additionally increase the riming and WBF terms. If the glaciation adjustment includes an adjustment in glaciation state, it may reduce the liquid adjustment to the autoconversion term. The overall effect of microphysical adjustments is to increase total as compared to partial susceptibility. Susceptibility will have low absolute values because the negative effect of droplet number changes on the collection processes riming and autoconversion competes with the positive effect on vapor deposition and glaciation. Additionally, contributions of nonsusceptible processes, namely accretion and aggregation, decrease susceptibility by increasing PP in Eq. (46). The sign of mixed-phase precipitation susceptibility to droplet number perturbations depends on the detailed composition of the cloud, that is, the relative importance of precipitation formation processes and the glaciation fraction in the region of dominant precipitation production.

To discuss the susceptibility to crystal number, we combine snow and graupel aggregation with ice–rain riming as agg, again using average values from Table 5:

$$\frac{d\ln \mathrm{PP}}{d\ln N_{ci}} > \frac{\partial \ln \mathrm{PP}}{\partial \ln N_{ci}} \approx -0.3\frac{\mathrm{agg}}{\mathrm{PP}} + 0.1\frac{\mathrm{self}}{\mathrm{PP}}. \quad (47)$$

Susceptibility is increased by glaciation adjustments as the aggregation term becomes less negative and the self-collection term is enhanced. As glaciation adjustments to crystal number perturbations are assumed to be strong in comparison to the glaciation adjustments to droplet number perturbations that are relevant for Eq. (46), overcompensation and overall positive precipitation susceptibility is likely, especially for strong

glaciation adjustments at low glaciation fractions. Observational evidence of positive precipitation susceptibility from glaciation adjustments at zero glaciation fraction is manifested in hole-punch clouds: Airplane-induced seeding of supercooled stratiform clouds with ice particles leads to the formation of larger hydrometeors and the local dissipation of the cloud (Heymsfield et al. 2011). Our analysis is in agreement with the glaciation indirect effect by explaining positive precipitation susceptibilities to crystal number perturbations by glaciation adjustments. It does not exclude negative precipitation susceptibilities, however, when aggregation and/or ice–rain riming dominate precipitation formation at intermediate or high glaciation fractions and weaker glaciation adjustments. In the limit of high glaciation fractions, Eq. (47) describes the precipitation susceptibility of ice clouds.

Aerosol perturbations to mixed-phase clouds affect the droplet activation as well as the ice-nucleation ability of particles. The resulting effect is obtained by weighting the individual susceptibilities of droplet and crystal number by their relative changes:

$$d\ln\mathrm{PP} = \frac{d\ln\mathrm{PP}}{d\ln N_{\mathrm{cl}}} d\ln N_{\mathrm{cl}} + \frac{d\ln\mathrm{PP}}{d\ln N_{\mathrm{ci}}} d\ln N_{\mathrm{ci}}. \qquad (48)$$

If droplet-activation and ice-nucleation-active aerosol are increased in parallel (e.g., by adding sulfate coated dust), effects on the warm pathway via autoconversion and riming are compensated by effects on the ice-phase pathway via aggregation and WBF-driven glaciation adjustment. When perturbations of the two aerosol characteristics have opposite signs (e.g., after additional ageing and partial removal of the coated dust from the previous example), the effects of both pathways enhance each other.

For an enhancing perturbation with $d\ln N := d\ln N_{\mathrm{ci}} = -d\ln N_{\mathrm{cl}}$, the precipitation signal is given by

$$\frac{d\ln\mathrm{PP}}{d\ln N} \approx 2.0\frac{\mathrm{aut}}{\mathrm{PP}} + 0.5\frac{\mathrm{rim}}{\mathrm{PP}} - 0.4\frac{\mathrm{pWBF}}{\mathrm{PP}} - \mathrm{adj} + 0.1\frac{\mathrm{self}}{\mathrm{PP}} - 0.3\frac{\mathrm{agg}}{\mathrm{PP}} + \mathrm{glac}, \qquad (49)$$

where adj and glac denote liquid and glaciation adjustments. The signal is optimized when accretion as nonsusceptible process and aggregation as a process acting against the glaciation effect are weak. This is the case for a nonprecipitating cloud. The absence of snow and graupel also removes the negative pWBF contribution. According to Figs. 3 and 5 the susceptibility of ice–droplet riming and self-collection increases in magnitude for very small droplets and crystals, respectively. Both are found for high aerosol backgrounds of droplet-activating and ice-nucleating aerosol. Continental aerosol conditions are generally more polluted than maritime ones. To detect an aerosol effect on precipitation, we thus propose to investigate the onset of precipitation from continental mixed-phase stratus for aerosol conditions that cross over from dust to industrially dominated conditions.

5. Summary and conclusions

We have analytically studied the susceptibility of precipitation production, which is directly related to the susceptibility of the precipitation rate [Eq. (12)]. Our discussion is based on the process rate equations in the two-moment, five-hydrometeor-category microphysics scheme of SB. As a bulk scheme, it has the advantage over a bin scheme of being analytically accessible. Conversion rates in the scheme are directly derived from the stochastic collection equation, and it has been validated against the operational version of the numerical weather prediction model COSMO (Baldauf et al. 2011). Based on the SB microphysics scheme, we estimate precipitation susceptibilities for warm and mixed- and ice-phase clouds taking into account microphysical adjustments.

The analysis presented can be adapted to other bulk microphysics schemes. The specific process susceptibilities will be characteristic to each scheme and could provide a versatile tool for evaluation and comparison, complementing the numerical analysis of warm precipitation susceptibilities from different schemes by Hill et al. (2015). The qualitative results discussed in the article that are rooted in basic physical mechanisms would be expected to emerge from most microphysics schemes. It would be interesting to see the analysis extended.

For the SB scheme, we qualitatively confirm previous studies and find warm precipitation susceptibility to be negative with compensating contributions from increasing cloud liquid and insensitivity of the accretion process [Eq. (42)]. For cirrus clouds, the sedimentation of crystals is treated as a precipitation analog. When taking into account adjustments in supersaturation, cirrus sedimentation susceptibility to crystal number reduces to the negative of the exponent of sedimentation velocity [Eq. (45)]. This negative value is qualitatively consistent with effects of cirrus seeding that are discussed in the literature (Mitchell and Finnegan 2009; Storelvmo and Herger 2014; Penner et al. 2015). For mixed-phase clouds, we in general expect low susceptibility values [Eqs. (46) and (47)] and apply the susceptibility framework to identify several microphysical

factors discussed in the following that contribute to these low values:

(i) Involvement of nonsusceptible processes. The relevance of accretion as nonsusceptible process has been discussed for warm clouds [e.g., by Sorooshian et al. (2009); Wood et al. (2009); Sant et al. (2015)]. Given the larger number of processes contributing to precipitation production in mixed-phase clouds [Eq. (14)], the relative contribution of susceptible processes can be reduced as compared to warm clouds.

(ii) Low partial susceptibilities of involved processes. We derived the partial susceptibilities of autoconversion, accretion, riming, aggregation, ice self-collection, and diffusional growth, including the WBF process, to the first and second moment (i.e., mass and number) of all involved hydrometeors (Table 5). We find that autoconversion is the most susceptible process with a negative quadratic dependence on droplet number and positive dependence to the fourth power on cloud liquid amount. The latter is comparably high for SB microphysics (Wood 2005). The susceptibilities of mixed- and ice-phase processes to changes in droplet and crystal number are distinctly lower than for the liquid phase, and scaling is not stronger than a square root. The differences in susceptibility follow from the sensitivity of the collection kernel to hydrometeor size. Droplet–riming susceptibility is determined by the collection efficiency. This is in agreement with previous studies that observed significant sensitivities of riming rate to the formulation of collection efficiency (Lohmann 2004; Saleeby and Cotton 2008). The decisive influence of collection kernels and efficiencies on susceptibilities stresses a need for better experimental constraints of these factors.

(iii) Compensating contributions of involved processes. Droplet-number susceptibility of mixed-phase precipitation productions is reduced because autoconversion and riming become less effective with increasing droplet number while the WBF process increases efficiency [Eq. (46)]. This effect was modeled in orographic clouds by Saleeby and Cotton (2013). For crystal-number susceptibility, ice self-collection becomes more effective with increasing crystal number, while aggregation with snow and graupel and ice–rain riming becomes less effective [Eq. (47)].

(iv) Compensating adjustments of cloud ice and liquid water to droplet and crystal number perturbations. We find that susceptibilities to masses are generally larger than to numbers (Table 5), indicating that precipitation susceptibilities are strongly influenced by adjustments or, equivalently, meteorological variability. We argue that microphysical processes alone tend to result in positive correlations between changes in droplet (crystal) number and cloud liquid (ice) water content. Such adjustments will compensate number effects on autoconversion, riming, and aggregation (Table 6). For intermediate glaciation fractions, droplet riming and WBF rates are additionally found robust to adjustments in the glaciation state of the cloud (Table 7).

(v) Negative feedback from sublimation of snow. Evaporation and sublimation of hydrometeors below cloud base is increased for increasing precipitation and thus poses a negative feedback reducing the absolute value of precipitation susceptibility. The effect is more important for snowflakes than for raindrops and reduces mixed-phase susceptibility more than warm susceptibility (Borys et al. 2003; Saleeby et al. 2009, 2011).

(vi) Compensations between simultaneous aerosol effects on ice-crystal and cloud-droplet number. Our analysis confirms previous studies on compensating effects of simultaneous increases in crystal and droplet number. In accordance with the glaciation indirect effect (Lohmann 2002; Lohmann and Hoose 2009), we find that the opposing effects on the warm and cold pathway of precipitation formation are not based on opposing responses of warm- and cold-phase collection processes but require glaciation adjustments in the cloud.

The compensating mechanisms discussed illustrate a range of possible contributions of cloud microphysics to dampening the aerosol signal in mixed-phase precipitation. All or some of them can occur but do not have to dominate in individual clouds and might be least active before the onset of precipitation in continental mixed-phase clouds. Especially in convective mixed-phase clouds, dynamical, thermodynamical, and radiative effects might lead to adjustments that are opposed to the microphysical adjustments assumed for our analysis. Discussing these adjustments is beyond the scope of this work. Other approaches, in particular numerical models that capture the complex interplay between microphysics and dynamics, are required to address these questions. Nevertheless, the plurality of options increases the probability of encountering additional buffering in mixed-phase as opposed to warm- and ice-phase clouds and thus provides evidence for the buffering hypothesis as a possible explanation for ambiguous and weak aerosol signals in continental precipitation.

Acknowledgments. This work was funded by the ETH-domain CCES project OPTIWARES (41-02). The authors thank the anonymous reviewers for their constructive comments.

APPENDIX

List of Symbols

$\cdot_{ci}$	Index denoting cloud ice category in SB
$\cdot_{cl}$	Index denoting cloud droplet category in SB
$\cdot_{l}$	Index denoting larger hydrometeor that collects another hydrometeor in a cold-phase collection process
$\cdot_{pg}$	Index denoting graupel category in SB
$\cdot_{pr}$	Index denoting rain category in SB
$\cdot_{ps}$	Index denoting snow category in SB
$\cdot_{s}$	Index denoting smaller hydrometeor that is collected in a cold-phase collection process
$\cdot_{x}$	Placeholder index, $x \in \{\text{cl, ci, pr, ps, pg, } s, l\}$
a_x	Prefactor in diameter–mass relationship of hydrometeor category x
acc	Mass accretion rate
adj	Adjustments in cloud liquid amount
agg	Mass aggregation rate (includes is-agg, ig-agg, and ir-rim)
aut	Mass autoconversion rate
b_x	Exponent in diameter–mass relationship of hydrometeor category x
ci-diff	Vapor deposition rate on cloud ice
coll	Mass collection rate of cold-phase process (represents rim, agg, and self)
d_1	Constant in ventilation coefficient
d_2	Constant in ventilation coefficient
diff	Net rate of vapor exchange with precipitation (includes ci-diff for cirrus; pr-, ps-, and pg-diff for mixed phase; and pr-diff for warm clouds)
$D_{\text{max,cl}}$	Droplet diameter above which $E_{\text{ic-rim}} = 1$
$D_{\text{min},x}$	Onset diameter of effective collection for hydrometeors in category x
D_x	(Equivalent) diameter of hydrometeor category x
e_1	Constant in autoconversion rate
e_2	Constant in autoconversion rate
e_3	Constant in accretion rate
E	Cold-phase collection efficiency
$E_{\text{ic-rim}}$	Collection efficiency of ice-droplet riming
f	Geometric part of cold-phase collection kernel
f_D	Diameter term of cold-phase collection kernel
f_v	Fall speed term of cold-phase collection kernel
F	Ventilation coefficient
gc-rim	Graupel-droplet riming rate (mass)
glac	Glaciation adjustment
ic-rim	Ice–droplet riming rate (mass)
ig-agg	Ice–graupel aggregation rate (mass)
ir-rim	Ice–rain riming rate (mass)
is-agg	Ice–snow aggregation rate (mass)
I	Total cloud water content in ice phase
L	Total cloud water content in liquid phase
M_x	Cloud water content in hydrometeor category x
N_x	Number of hydrometeors in category x
pg-diff	Vapor deposition rate on graupel
pr-diff	Vapor deposition rate on rain
ps-diff	Vapor deposition rate on snow
P	Precipitation rate (sedimentation rate for cirrus clouds)
P_{ice}	Sedimentation rate of ice crystals from cirrus clouds
PP	Precipitation production, especially in mixed-phase clouds
PP_{ice}	Production rate of M_{ci} in cirrus clouds
PP_{warm}	Precipitation production of warm rain
r	Mass change by microphysical process, $r \in R$
rim	Droplet-riming rate (includes ic-, sc-, and gc-rim)
R	List of mass rates of change from microphysical processes aut, acc, rim, agg, and diff
s	Total precipitation susceptibility
sc-rim	Snow–droplet riming rate (mass)
self	Ice–ice self-collection rate (mass)
v_x	Terminal fall speed of hydrometeor category x
pWBF	Mass transfer rate by Wegener–Bergeron–Findeisen process with vapor deposition on snow and graupel (but not on ice)
x_x	Average mass of hydrometeor in class x
x_{min}	Minimum average mass required for a microphysical process (corresponds to $D_{\text{min},x}$ for coll and to the minimum average mass defining the hydrometeor category for x-diff)
x_{max}	Maximum average mass defining a hydrometeor category
x-diff	Vapor deposition on hydrometeor category x
X	Prognostic moment of SB scheme (i.e., M_x or N_x)
Y	Prognostic moment of SB scheme (i.e., M_x or N_x)
α_x	Prefactor in fall speed–mass relationship of hydrometeor category x
β_x	Exponent in fall speed–mass relationship of hydrometeor category x
γ	Fraction of total cloud water in ice phase
Γ	Generalized gamma function
$\delta_{x,k}$	Integration factor in f_D
$\delta_{y,x,k}$	Integration factor in f_D
ε	Fraction of total cloud liquid in rain category
$\theta_{x,k}$	Integration factor in f_v
$\theta_{y,x,k}$	Integration factor in f_v

μ_x Parameter of Γ
ν_x Parameter of Γ
σ_x Variance of fall-velocity distribution of hydrometeor category x
Φ_{cc} Scaling function in autoconversion rate
Φ_{cr} Scaling function in accretion rate

REFERENCES

Albrecht, B. A., 1989: Aerosols, cloud microphysics, and fractional cloudiness. *Science*, **245**, 1227–1230, doi:10.1126/science.245.4923.1227.

Baldauf, M., A. Seifert, J. Forstner, D. Majewski, and M. Raschendorfer, 2011: Operational convective-scale numerical weather prediction with the COSMO model: Description and sensitivities. *Mon. Wea. Rev.*, **139**, 3887–3905, doi:10.1175/MWR-D-10-05013.1.

Bangert, M., C. Kottmeier, B. Vogel, and H. Vogel, 2011: Regional scale effects of the aerosol cloud interaction simulated with an online coupled comprehensive chemistry model. *Atmos. Chem. Phys.*, **11**, 4411–4423, doi:10.5194/acp-11-4411-2011.

Bergeron, T., 1935: On the physics of cloud and precipitation. *Procès-Verbaux des Séances de L'Association de Météorologie: Cinquième Assemblée Générale*, Vol. II, International Union of Geodesy and Geophysics, 156–178.

Borys, R. D., D. H. Lowenthal, S. A. Cohen, and W. O. J. Brown, 2003: Mountaintop and radar measurements of anthropogenic aerosol effects on snow growth and snowfall rate. *Geophys. Res. Lett.*, **30**, 1538, doi:10.1029/2002GL016855.

Boucher, O., and Coauthors, 2013: Clouds and aerosols. *Climate Change 2013: The Physical Science Basis*, T. F. Stocker et al., Eds., Cambridge University Press, 571–658, doi:10.1017/CBO9781107415324.016.

Duong, H. T., A. Sorooshian, and G. Feingold, 2011: Investigating potential biases in observed and modeled metrics of aerosol–cloud–precipitation interactions. *Atmos. Chem. Phys.*, **11**, 4027–4037, doi:10.5194/acp-11-4027-2011.

Feingold, G., and H. Siebert, 2009: Cloud–aerosol interactions from the micro to the cloud scale. *Clouds in the Perturbed Climate System*, J. Heintzenberg and R. J. Charlson, Eds., MIT Press, 319–338, doi:10.7551/mitpress/9780262012874.003.0014.

——, A. McComiskey, D. Rosenfeld, and A. Sorooshian, 2013: On the relationship between cloud contact time and precipitation susceptibility to aerosol. *J. Geophys. Res. Atmos.*, **118**, 10 544–10 554, doi:10.1002/jgrd.50819.

Findeisen, W., 1938: Die kolloidmeteorologischen Vorgänge bei der Niederschlagsbildung (Colloidal meteorological processes in the formation of precipitation). *Meteor. Z.*, **55**, 121–133.

Gettelman, A., H. Morrison, C. R. Terai, and R. Wood, 2013: Microphysical process rates and global aerosol–cloud interactions. *Atmos. Chem. Phys.*, **13**, 9855–9867, doi:10.5194/acp-13-9855-2013.

Glassmeier, F., 2016: Constraining susceptibilities of aerosol–cloud–precipitation interactions in warm and cold clouds. Ph.D. thesis, ETH Zürich, 126 pp., doi:10.3929/ethz-a-010614474.

Heymsfield, A. J., G. Thompson, H. Morrison, A. Bansemer, R. M. Rasmussen, P. Minnis, and Z. W. D. Zhang, 2011: Formation and spread of aircraft-induced holes in clouds. *Science*, **333**, 77–81, doi:10.1126/science.1202851.

Hill, A. A., B. J. Shipway, and I. A. Boutle, 2015: How sensitive are aerosol–precipitation interactions to the warm rain response? *J. Adv. Model. Earth Syst.*, **7**, 987–1004, doi:10.1002/2014MS000422.

Jiang, H., G. Feingold, and A. Sorooshian, 2010: Effect of aerosol on the susceptibility and efficiency of precipitation in warm trade cumulus clouds. *J. Atmos. Sci.*, **67**, 3525–3540, doi:10.1175/2010JAS3484.1.

Kärcher, B., and U. Lohmann, 2003: A parameterization of cirrus cloud formation: Heterogeneous freezing. *J. Geophys. Res.*, **108**, 4402, doi:10.1029/2002JD003220.

Khairoutdinov, M., and Y. Kogan, 2000: A new cloud physics parameterization in a large-eddy simulation model of marine stratocumulus. *Mon. Wea. Rev.*, **128**, 229–243, doi:10.1175/1520-0493(2000)128<0229:ANCPPI>2.0.CO;2.

Korolev, A., 2007: Limitations of the Wegener–Bergeron–Findeisen mechanism in the evolution of mixed-phase clouds. *J. Atmos. Sci.*, **64**, 3372–3375, doi:10.1175/JAS4035.1.

Krämer, M., and Coauthors, 2009: Ice supersaturations and cirrus cloud crystal numbers. *Atmos. Chem. Phys.*, **9**, 3505–3522, doi:10.5194/acp-9-3505-2009.

Kuebbeler, M., U. Lohmann, J. Hendricks, and B. Kärcher, 2014: Dust ice nuclei effect on cirrus clouds. *Atmos. Chem. Phys.*, **14**, 3027–3046, doi:10.5194/acp-14-3027-2014.

Lebo, Z. J., and G. Feingold, 2014: On the relations between responses in cloud water and precipitation to changes in aerosol. *Atmos. Chem. Phys.*, **14**, 11 817–11 831, doi:10.5194/acp-14-11817-2014.

Lohmann, U., 2002: A glaciation indirect aerosol effect caused by soot aerosols. *Geophys. Res. Lett.*, **29**, 1052, doi:10.1029/2001GL014357.

——, 2004: Can anthropogenic aerosols decrease the snowfall rate? *J. Atmos. Sci.*, **61**, 2457–2468, doi:10.1175/1520-0469(2004)061<2457:CAADTS>2.0.CO;2.

——, and C. Hoose, 2009: Sensitivity studies of different aerosol indirect effects in mixed-phase clouds. *Atmos. Chem. Phys.*, **9**, 8917–8934, doi:10.5194/acp-9-8917-2009.

Long, A. B., and M. J. Manton, 1974: On the evolution of the collection kernel for the coalescence of water droplets. *J. Atmos. Sci.*, **31**, 1053–1057, doi:10.1175/1520-0469(1974)031<1053:OTEOTC>2.0.CO;2.

Lu, M.-L., A. Sorooshian, H. H. Jonsson, G. Feingold, R. C. Flagan, and J. H. Seinfeld, 2009: Marine stratocumulus aerosol–cloud relationships in the MASE-II experiment: Precipitation susceptibility in eastern Pacific marine stratocumulus. *J. Geophys. Res.*, **114**, D24203, doi:10.1029/2009JD012774.

McComiskey, A., and G. Feingold, 2012: The scale problem in quantifying aerosol cloud indirect effects. *Atmos. Chem. Phys.*, **12**, 1031–1049, doi:10.5194/acp-12-1031-2012.

Mitchell, D. L., and W. Finnegan, 2009: Modification of cirrus clouds to reduce global warming. *Environ. Res. Lett.*, **4**, 045102, doi:10.1088/1748-9326/4/4/045102.

Muhlbauer, A., T. Hashino, L. Xue, A. Teller, U. Lohmann, R. M. Rasmussen, I. Geresdi, and Z. Pan, 2010: Intercomparison of aerosol–cloud–precipitation interactions in stratiform orographic mixed-phase clouds. *Atmos. Chem. Phys.*, **10**, 8173–8196, doi:10.5194/acp-10-8173-2010.

Mülmenstädt, J., O. Sourdeval, J. Dalanoë, and J. Quaas, 2015: Frequency of occurrence of rain from liquid-, mixed-, and ice-phase clouds derived from A-Train satellite retrievals. *Geophys. Res. Lett.*, **42**, 6502–6509, doi:10.1002/2015GL064604.

Myhre, G., and Coauthors, 2013: Anthropogenic and natural radiative forcing. *Climate Change 2013: The Physical Science Basis*, T. F. Stocker, et al., Eds., Cambridge University Press, 659–740, doi:10.1017/CBO9781107415324.018.

Noppel, H., U. Blahak, A. Seifert, and K. D. Beheng, 2010: Simulations of a hailstorm and the impact of CCN using an advanced two-moment cloud microphysical scheme. *Atmos. Res.*, **96**, 286–301, doi:10.1016/j.atmosres.2009.09.008.

Penner, J. E., C. Zhou, and X. Liu, 2015: Can cirrus cloud seeding be used for geoengineering? *Geophys. Res. Lett.*, **42**, 8775–8782, doi:10.1002/2015GL065992.

Saleeby, S. M., and W. R. Cotton, 2008: A binned approach to cloud-droplet riming implemented in a bulk microphysics model. *J. Appl. Meteor. Climatol.*, **47**, 694–703, doi:10.1175/2007JAMC1664.1.

——, and ——, 2013: Aerosol impacts on the microphysical growth processes in orographic snowfall. *J. Appl. Meteor. Climatol.*, **52**, 834–852, doi:10.1175/JAMC-D-12-0193.1.

——, ——, D. Lowenthal, R. D. Borys, and M. A. Wetzel, 2009: Influence of cloud condensation nuclei on orographic snowfall. *J. Appl. Meteor. Climatol.*, **48**, 903–922, doi:10.1175/2008JAMC1989.1.

——, ——, and J. D. Fuller, 2011: The cumulative impact of cloud droplet nucleating aerosols on orographic snowfall in Colorado. *J. Appl. Meteor. Climatol.*, **50**, 604–625, doi:10.1175/2010JAMC2594.1.

Sant, V., R. Posselt, and U. Lohmann, 2015: Prognostic precipitation with three liquid water classes in the ECHAM5–HAM GCM. *Atmos. Chem. Phys.*, **15**, 8717–8738, doi:10.5194/acp-15-8717-2015.

Seifert, A., and K. D. Beheng, 2001: A double-moment parameterization for simulating autoconversion, accretion and self-collection. *Atmos. Res.*, **59–60**, 265–281, doi:10.1016/S0169-8095(01)00126-0.

——, and ——, 2006: A two-moment cloud microphysics parameterization for mixed-phase clouds. Part 1: Model description. *Meteor. Atmos. Phys.*, **92**, 45–66, doi:10.1007/s00703-005-0112-4.

——, C. Köhler, and K. D. Beheng, 2012: Aerosol–cloud–precipitation effects over Germany as simulated by a convective-scale numerical weather prediction model. *Atmos. Chem. Phys.*, **12**, 709–725, doi:10.5194/acp-12-709-2012.

Sherwood, S. C., S. Bony, O. Boucher, C. Bretherton, P. M. Forster, J. M. Gregory, and B. Stevens, 2015: Adjustments in the forcing-feedback framework for understanding climate change. *Bull. Amer. Meteor. Soc.*, **96**, 217–228, doi:10.1175/BAMS-D-13-00167.1.

Sorooshian, A., G. Feingold, M. D. Lebsock, H. Jiang, and G. L. Stephens, 2009: On the precipitation susceptibility of clouds to aerosol perturbations. *Geophys. Res. Lett.*, **36**, L13803, doi:10.1029/2009GL038993.

Stevens, B., and A. Seifert, 2008: Understanding macrophysical outcomes of microphysical choices in simulations of shallow cumulus convection. *J. Meteor. Soc. Japan*, **86A**, 143–163, doi:10.2151/jmsj.86A.143.

——, and G. Feingold, 2009: Untangling aerosol effects on clouds and precipitation in a buffered system. *Nature*, **461**, 607–613, doi:10.1038/nature08281.

Stjern, C. W., and J. E. Kristjánsson, 2015: Contrasting influences of recent aerosol changes on clouds and precipitation in Europe and East Asia. *J. Climate*, **28**, 8770–8790, doi:10.1175/JCLI-D-14-00837.1.

Storelvmo, T., and N. Herger, 2014: Cirrus cloud susceptibility to the injection of ice nuclei in the upper troposphere. *J. Geophys. Res. Atmos.*, **119**, 2375–2389, doi:10.1002/2013JD020816.

——, J. E. Kristjánsson, U. Lohmann, T. Iversen, A. Kirkevag, and O. Seland, 2008: Modeling of the Wegener–Bergeron–Findeisen process—Implications for aerosol indirect effects. *Environ. Res. Lett.*, **3**, 045001, doi:10.1088/1748-9326/3/4/045001.

Terai, C. R., R. Wood, D. C. Leon, and P. Zuidema, 2012: Does precipitation susceptibility vary with increasing cloud thickness in marine stratocumulus? *Atmos. Chem. Phys.*, **12**, 4567–4583, doi:10.5194/acp-12-4567-2012.

——, ——, and T. L. Kubar, 2015: Satellite estimates of precipitation susceptibility in low-level marine stratiform clouds. *J. Geophys. Res. Atmos.*, **120**, 8878–8889, doi:10.1002/2015JD023319.

Twomey, S., 1974: Pollution and the planetary albedo. *Atmos. Environ.*, **8**, 1251–1256, doi:10.1016/0004-6981(74)90004-3.

Wegener, A., 1911: *Thermodynamik der Atmosphäre*. Johann Ambrosius Barth, 331 pp.

Wood, R., 2005: Drizzle in stratiform boundary layer clouds. Part II: Microphysical aspects. *J. Atmos. Sci.*, **62**, 3034–3050, doi:10.1175/JAS3530.1.

——, T. L. Kubar, and D. L. Hartmann, 2009: Understanding the importance of microphysics and macrophysics for warm rain in marine low clouds. Part II: Heuristic models of rain formation. *J. Atmos. Sci.*, **66**, 2973–2990, doi:10.1175/2009JAS3072.1.